A team of heterochromatin factors collaborates with small RNA pathways to combat repetitive elements and germline stress

Alicia N. McMurchy[1], Przemyslaw Stempor[1], Tessa Gaarenstroom[1], Brian Wysolmerski, Yan Dong, Darya Aussianikava, Alex Appert, Ni Huang, Paulina Kolasinska-Zwierz, Alexandra Sapetschnig, Eric Miska, and Julie Ahringer*

The Gurdon Institute and Department of Genetics, University of Cambridge, Cambridge UK

[1]equal contribution

*author for correspondence (j.ahringer@gurdon.cam.ac.uk)

Abstract

Repetitive sequences derived from transposons make up a large fraction of eukaryotic genomes and must be silenced to protect genome integrity. Repetitive elements are often found in heterochromatin; however, the roles and interactions of heterochromatin proteins in repeat regulation are poorly understood. Here we show that a diverse set of *C. elegans* heterochromatin proteins act together with the piRNA and nuclear RNAi pathways to silence repetitive elements and prevent genotoxic stress in the germ line. Mutants in genes encoding HPL-2/HP1, LIN-13, LIN-61, LET-418/Mi-2, and H3K9me2 histone methyltransferase MET-2/SETDB1 also show functionally redundant sterility, increased germline apoptosis, DNA repair defects, and interactions with small RNA pathways. Remarkably, fertility of heterochromatin mutants could be partially restored by inhibiting *cep-1*/p53, endogenous meiotic double strand breaks, or the expression of MIRAGE1 DNA transposons. Functional redundancy among these factors and pathways underlies the importance of safeguarding the genome through multiple means.

Introduction

Heterochromatin, the more tightly packed form of chromatin, plays important roles in maintaining the structural and functional integrity of the genome (1). It is less transcriptionally active than euchromatin and highly enriched for repetitive elements such as transposons and satellite repeats, which are kept silent to maintain genome integrity. The heterochromatin state is stable and heritable across generations highlighting the importance of keeping certain regions of the genome repressed.

Histones in heterochromatin are marked with modifications associated with transcriptional repression such as H3K9 methylation. In organisms with point centromeres, heterochromatin is typically found in large domains adjacent to centromeres and telomeres (1). In *C. elegans*, heterochromatin associated histone methylations H3K9me2 and H3K9me3 are instead mostly found in many small domains on the distal arm regions of autosomal chromosomes (2). This pattern is likely to be related to the holocentric nature of *C. elegans* chromosomes, which have distributed centromeres rather than a single point centromere. Two histone methyltransferases carry out all H3K9 methylation (3). The SETDB1 homolog MET-2 carries out mono- and di-methylation of H3K9. SET-25 primarily carries out tri-methylation of H3K9, but it can generate all three methylated forms of H3K9. In the absence of both proteins, H3K9 methylation is undetectable, heterochromatic distal arm regions show reduced association with the nuclear lamina, and heterochromatic transgenes are desilenced (3).

A hallmark of heterochromatin is heterochromatin protein 1 (HP1), the first heterochromatin protein to be discovered through work in Drosophila (4, 5). HP1 contains a chromodomain that binds to methylated H3K9, and it is essential for

heterochromatin maintenance (4). In addition to HP1, a large and diverse array of proteins is associated with heterochromatin, including nucleosome remodelers, histone modifying enzymes, histone binding proteins, and DNA binding proteins (6, 7). However the functions and interactions of heterochromatin proteins are not well understood.

Many *C. elegans* proteins that have predicted functions in heterochromatin or transcriptional repression are important for development. These include MET-2/SETDB1, HPL-2/HP1, LIN-61, LIN-13, and LET-418/Mi-2 (8-13). HPL-2 is a *C. elegans* ortholog of heterochromatin HP1, and LIN-61 is a protein containing MBT (malignant brain tumor) repeats. Both HPL-2 and LIN-61 can bind to all methylated forms of H3K9 *in vitro* (12, 14, 15), and both can repress a heterochromatic reporter (3, 8, 16). LIN-13 is a multi-zinc finger protein (10). A complex containing LIN-13, HPL-2, and LIN-61 has been detected *in vivo*, and LIN-13 is required for the formation of HPL-2::GFP nuclear foci (13, 17). LET-418 is an ortholog of Mi-2, an ATP-dependent nucleosome remodelling component of the repressive NuRD and Mec complexes (9, 18, 19).

Mutants of *hpl-2*, *lin-61*, *lin-13*, *met-2*, and *let-418* display both germ line and somatic defects. *let-418* and *lin-13* null mutants are sterile (9, 10), *hpl-2* null mutants show temperature sensitive sterility (11), and *lin-61* and *met-2* null mutants have slightly reduced brood sizes (12). The underlying cause of the fertility defects is not known, but *hpl-2* mutants have been shown to produce abnormal oocytes, suggesting defective gametogenesis (8). Somatic defects are pleiotropic and show similarities among mutants, with most showing slow growth, somatic expression of germ line genes, synthetic vulval development defects, and larval arrest (some only at high temperature) (10, 11, 13, 16-18, 20-23). Additionally, genetic interactions have been

observed between some of the mutants, suggesting partially redundant functions, and that defects may result from alteration of a shared heterochromatin-linked process (12, 17, 24).

The genomic distribution of only one of the above heterochromatin proteins has been studied. An HPL-2 ChIP-chip study in early embryos showed that most binding was on the distal arm regions of autosomes in a pattern of similar to H3K9me1 and H3K9me2; interestingly, binding to chromatin was not dependent on H3K9 methylation (14). HPL-2 was observed to be broadly genic, with additional association at promoters in central chromosome regions and at repeats on distal arm regions; however, no clear relationship between HPL-2 binding and gene expression changes was observed (14). Systematic and comparative analyses of heterochromatin factors are needed to understand their functions.

The genomic binding patterns of orthologs of some of the above factors suggest roles in the regulation of mobile elements. SETDB1 binds to promoters of developmentally regulated genes in mammalian embryonic stem cells, 40% of which are found next to or overlapping endogenous retroviruses (25-27). In addition, retrotransposons are derepressed in *Setdb1* knockout mouse ES cell lines and primordial germ cells (26, 28). Retrotransposons are also repressed by HP1α and HP1β in mESCs, but it is a different set of retrotransposons than is targeted by SETDB1 (29). Drosophila HP1 binds to genes and to transposable elements, particularly in pericentric chromosomal regions, but transposable element expression in mutants has not been assessed (30, 31). A recent study showed that Mi-2 could bind to a LINE1 retrotransposon promoter and repress a LINE1 reporter in human and mouse cell lines (32). The genomic distribution of Mi-2 is unclear as different genome-wide binding studies in human ES cells have yielded conflicting results (33).

The expression of repetitive elements can be detrimental to genome stability due to the negative effects of homologous recombination and transposon-induced breaks. Because the germline produces the gametes that transmit genetic information across generations, silencing of repetitive elements is an absolute requirement for germ line health. A small RNA pathway called the piRNA pathway, present in most animals, plays a role in transposon silencing in the germ line (34). Recent work in *C. elegans* implicated HPL-2/HP1 and the H3K9me3 histone methyltransferase SET-25 in piRNA pathway function, indicating a connection between heterochromatin and small RNA silencing of piRNA targets (35).

In the *C. elegans* germ line, the piRNA pathway involves generation of 21nt piRNAs that bind to the Piwi argonaute protein PRG-1 (36-38). This triggers generation of secondary 22G siRNAs that mediate silencing either in the cytoplasm or nucleus (35, 37, 39-47). Cytoplasmic silencing mechanisms are not well understood, but recent advances have been made in the understanding of transcriptional silencing. In the nucleus, the piRNA pathway engages a second small RNA pathway called the nuclear RNAi pathway, which orchestrates H3K9 and H3K27 methylation and/or inhibition of RNA Pol II (42, 46, 48, 49). Although the nrde pathway can be triggered by the piRNA pathway in the germ line, it is also active in the soma, with dedicated Argonaute proteins for germ line (HRDE-1) and soma (NRDE-3) (42, 46, 47, 50). Regions transcriptionally upregulated in *hrde-1* mutants were found to be enriched for retrotransposons, suggesting that repetitive elements may be endogenous targets in the germ line (51).

In addition to silencing transcription and maintaining the structural and functional integrity of the genome, heterochromatin also plays an important role in DNA repair. Heterochromatic compaction protects DNA from damage, and regulated

decondensation is important for damage repair (52). Additionally, in mammals, transient formation of heterochromatin occurs at the edges of double strand breaks, which involves recruitment of heterochromatin-associated proteins HP1 and nucleosome remodeller Mi-2, as well as methylation of H3K9 (53). This is thought to aid in damage repair by keeping the broken strands in proximity and inhibiting local transcription.

Here, through systematic genetic and genomic analyses, we investigate interactions and functions of five heterochromatin proteins (HPL-2/HP1, LIN-13, LIN-61, LET-418/Mi-2 and MET-2/SETDB1) and relationships with the piRNA and nuclear RNAi pathways. Our results reveal a nexus of factors that cooperate to prevent expression of repetitive elements and protect the germ line from endogenous damage.

Results

Heterochromatin factors show partially redundant functions for fertility

The five genes we study here (*hpl-2*/HP1, *lin-13*, *lin-61*, *let-418*/Mi-2, and *met-2*) are needed for normal fertility ((9-12, 54, 55); Supplementary file 1). Previous analyses uncovered genetic interactions in fertility between three pairs of genes (*hpl-2* and *lin-13*, *lin-61* and *hpl-2*, *lin-61* and *met-2*; (12, 17, 24); however, the remaining six combinations were untested. Using RNAi in mutant backgrounds, we found that double loss of function of each of the uninvestigated pairs also caused synthetic sterility, which we also observed for three tested double mutant combinations (Figures 1A-C). The single mutants show complex and pleiotropic germ line defects, but they all showed a high occurrence of abnormal oocytes, suggesting that sterility may be due in part to abnormal oogenesis (Figure 1-figure supplement 1). The fertility defects of single mutants and the enhancement in double loss of function combinations indicate that the five heterochromatin factors each have unique and partially redundant germ line roles. The genetic interactions suggest that the five factors may cooperate in a germ line process required for fertility.

HPL-2, LIN-13, LIN-61, LET-418, and MET-2 are enriched at repetitive elements and show extensive co-binding

To begin to investigate the roles of HPL-2, LIN-13, LIN-61, LET-418, and MET-2 in genome regulation, we mapped their binding locations using ChIP-seq analyses in young adults and compared the patterns to each other and to those of H3K9me2 and H3K9me3. Binding of each of the five factors is enriched on the distal arm regions of

the autosomes (Figure 2A; Figure 2-figure supplement 1A), as previously seen for H3K9me2, H3K9me3, and HPL-2 (2, 14, 56). Examination of ChIP-seq signals at a more local level revealed similar binding patterns for the five heterochromatin proteins (Figure 2B). Indeed, genome-wide correlation analyses showed significant positive correlations in signal between all datasets (Figure 2-figure supplement 1B). In addition, signals for each of the five heterochromatin factors showed high correlation with H3K9me2 but not with H3K9me3 (Figure 2B, Figure 2-figure supplement 1B).

To further investigate patterns of binding, we identified regions of peak enrichment for each dataset (Figure 2-figure supplement 1C, Figure 2-source data 1; 12449 to 19313 peaks per factor). For each factor, peaks are enriched on the distal chromosomal regions of autosomes; most peaks are intergenic or located in introns, with enrichment for intergenic binding in central chromosomal regions and enrichment for intronic binding in distal arm regions (Figure 2-figure supplement 1A).

To facilitate comparisons between datasets, we merged peak calls from all factors into a superset termed Any5 (n=33,301), then annotated each region in the Any5 set for the factors bound (Figure 2-source data 1). There is a high degree of peak overlap among the five factors, with 58% of sites in the Any5 set being bound by >1 factor (Figure 2C). Sites uniquely bound by only one factor are in the minority within each dataset (3.4%– 27.4%, Figure 2C and Figure 2-figure supplement 1C). Strikingly, the largest binding group contains all five factors (termed “All5”; Figure 2C). Enrichments for H3K9me2 and H3K9me3 vary between binding classes, with the All5 class showing high enrichment for H3K9me2 (Figure 2C). These results show that HPL-2, LET-418, LIN-13, LIN-61, and MET-2 extensively overlap in binding genome-wide.

The previous HPL-2 ChIP-chip study in embryos noted binding at repetitive elements, which are concentrated on the distal arm regions of autosomes (14). Repeat-rich heterochromatin in *C. elegans* is distributed in small domains rather than being concentrated in large regions as in mammals or Drosophila; therefore, the sequences of most repetitive regions have been determined. To investigate the association of heterochromatin factor binding at repetitive DNA, we used the recent Dfam2.0 annotation, which classified 62,331 individual repetitive elements in *C. elegans* into 184 repeat families, which were further classified by type (e.g., DNA transposon, retrotransposon, satellite, or unknown (57)).

We observed that HPL-2, LIN-13, LIN-61, LET-418, and MET-2 are all strongly associated with repetitive DNA elements (Figure 2C). A large proportion of each factor's peaks overlaps a repeat sequence (46.3% - 71.0%), and regions with all five factors have particularly strong repeat association (76.6%, Figure 2C, Figure 2-figure supplement 1C). Furthermore, of the total set of 62331 annotated repetitive elements, nearly half (46%) overlap a peak of at least one factor, and 8002 (13%) by all five factors (Figure 2-figure supplement 1D). All repeat types and 180 of 184 repeat families are associated with a heterochromatin factor peak; of these, 105 repeat families are enriched for binding by at least one factor (Figure 2-source data 2). HPL-2, LIN-13, LIN-61, MET-2, and H3K9me2 have a particularly strong association with Helitron families; LET-418 shows generally lower enrichment on repeat families than the other factors (Figure 2D; Figure 2-figure supplements 2-6).

H3K9me2 and H3K9me3 show different patterns of repeat enrichment. H3K9me2 is more associated with DNA transposons and satellite repeats, similar to the heterochromatin factors, whereas H3K9me3 is particularly associated with retrotransposon families, especially LINE and SINE elements (Figure 2D; Figure 2-

figure supplements 7-8). We also observed that H3K9me2 and all heterochromatin factors are enriched at telomeres, whereas H3K9me3 is not (Figure 2-figure supplement 1E). The binding and co-association of HPL-2, LET-418, LIN-13, LIN-61, and MET-2 at repetitive elements suggests roles in the regulation of these sequences.

Repetitive elements are desilenced in *hpl-2, lin-13, lin-61, let-418,* and *met-2 set-25* mutants

Because silencing of repetitive DNA elements is important for germ line function, we considered that the heterochromatin factors might function in preventing repeat expression. To investigate this possibility, we generated and analysed RNA sequence expression data for wild-type and heterochromatin mutant adults. MET-2 deposits H3K9me1 and H3K9me2, but all three methylation states of H3K9 are still present in *met-2* mutants (at lower levels) due to the action of SET-25 (3). Therefore we assayed a *met-2 set-25* double mutant, in which H3K9 methylation was not detectable (3). For each strain, we performed two biological replicates and differential expression analyses of the 62,331 Dfam2.0 repeat elements.

We observed upregulation of repetitive elements in every mutant strain (*hpl-2, let-418, lin-13, lin-61,* and *met-2 set-25*) (Figures 3A-D, Figure 3-figure supplement 1, Figure 3-source data 1). A total of 71 individual repeat elements representing 29 different families were upregulated in at least one mutant (Figure 3-source data 2; upregulation of 61/71 individual elements was confirmed based on uniquely mapping reads, see Methods). We observed a striking overlap in the sets of repetitive elements regulated by the heterochromatin factors: 41% of elements are upregulated in more

than one mutant (Figure 3A; Figure 3-source data 2). Furthermore, seven repeat elements are upregulated in all five strains, all of which are MIRAGE1 DNA transposable elements (Figures 3A, C, D, Figure 3-source data 2). The majority of repetitive elements upregulated in each heterochromatin mutant strain are DNA transposons, but retrotransposons are enriched for being upregulated (Figure 3B). Mutants show variation in the classes of repeats regulated; for example, SINE retrotransposons are particularly affected in *let-418* mutants, while many Helitron elements are upregulated in *lin-13* mutants (Figure 3B).

Overall, the total number of individual repetitive elements found with significantly altered expression is extremely small (<1%) relative to the >30,000 with factor binding, indicating that binding does not generally regulate repeat transcription. There are many types of repetitive elements, and only a small fraction would be expected to have potential for RNA expression. For example, 67% of repetitive elements are predicted to be non-autonomous DNA transposons, which would be mobilised in trans by a transposase encoded by another repetitive element, and many annotated elements are small fragments of larger elements. We therefore wondered whether the upregulation of repetitive element expression in heterochromatin mutants might be particularly associated with transposases or retrotransposons. Of 62331 Dfam2.0 elements, 221 overlap a predicted transposase ORF, and 1085 are annotated as LTR retrotransposons. We found that elements upregulated in any heterochromatin factor mutant are 83-fold enriched for containing a transposase (21 of 71) and 10-fold enriched for LTR retrotransposons (13 of 71), together accounting for nearly half of upregulated repeats. Therefore, a key role of heterochromatin factors is to suppress expression of repetitive element transposases. The widespread binding of heterochromatin factors to non-expressed repetitive elements is likely to play roles

other than in the regulation of transcription. These could include preventing the cutting, copying, or movement of elements, or maintaining genome integrity by supressing homologous recombination between repetitive elements (58, 59).

We also analysed alterations in protein coding gene expression in the heterochromatin mutants. Consistent with roles in repression, we identified three to five times more genes with upregulated expression in each mutant strain compared to those with reduced expression (267-513 upregulated genes per mutant; Figure 3-source data 3). Additionally, there is a high degree of overlap among the upregulated genes; of the total set of 1155 genes upregulated in any of the five mutant strains, 404 are upregulated in more than one (Figure 3-source data 3). Heterochromatin factors are enriched at upregulated genes, but not downregulated genes (except for genes misregulated in *let-418* mutants); additionally, both H3K9me2 and H3K9me3 are enriched at upregulated genes in all mutant strains (Figure 3-figure supplement 2). Enrichment for all factors and H3K9 methylation is particularly strong at genes upregulated in *met-2 set-25* mutants (Figure 3-figure supplement 2). These associations suggest direct roles in repression.

Repression of desilenced MIRAGE1 elements partially restores fertility of heterochromatin mutants.

The silencing of repetitive elements is a universal conserved feature of germ line function. The prominent upregulation of MIRAGE1 elements in all heterochromatin mutants prompted us to ask whether expression of this element might play a role in their reduced fertility. MIRAGE1 is an autonomous DNA transposable element that has two open reading frames. Of 69 MIRAGE1 element annotations in Dfam2.0, only

six are full length. These six, plus an additional six partial MIRAGE1 elements are upregulated in at least one heterochromatin mutant, and both ORFs show upregulation.

We first examined the tissue distribution of MIRAGE RNA using RNA-FISH (60). As expected from the RNA-seq results, wild-type adults had very low levels of MIRAGE1 RNA-FISH signal in germ line and soma (Figure 3E and Figure 3-figure supplement 3). In three tested heterochromatin mutants (*hpl-2*, *let-418*, and *lin-13*), we observed abundant germ line localized MIRAGE1 RNA whereas somatic expression remained low (Figure 3E and Figure 3-figure supplement 3). Therefore, *hpl-2*, *let-418*, and *lin-13* are important for repression of MIRAGE1 in the germ line.

To test whether upregulation of MIRAGE1 contributes to sterility, we used two sets of RNAi clones to simultaneously knockdown ORF1 and ORF2 (sets termed *mirage-A* and *mirage-B*). *mirage-A* and *mirage-B* target 16 different MIRAGE1 elements, including all full length elements and most of the MIRAGE1 elements upregulated in each of these mutants (8/8 for *let-418*, 7/8 for *lin-13*, and 10/11 for *hpl-2*). To assess an effect on fertility, we grew *hpl-2*, *lin-13*, and *let-418* mutants at 25°C, a condition under which they are nearly sterile, and tested for an increase in brood size after RNAi knockdown. Remarkably, RNAi of MIRAGE1 using *mirage-A* or *mirage-B* sets of RNAi clones led to a small but significant increase in fertility of all three mutants, showing that inappropriate MIRAGE1 expression contributes to their sterility (Figure 4A). We also observed that MIRAGE1 RNAi resulted in amelioration of somatic growth defects (not shown). These results indicate that one mechanism by which heterochromatin proteins promote normal germ line function is via the repression of repetitive elements, in particular those encoding transposases.

Heterochromatin mutants display DNA repair defects, increased germ line apoptosis and fertility dependence on CEP-1/p53

Desilencing of repetitive elements has been reported to cause DNA damage in other organisms (61); therefore, repeat expression in heterochromatin mutants might lead to genotoxic stress and genome instability in the germ line. Consistent with this, loss of *lin-61* leads to replication stress and genome instability, with increased germ line and somatic mutation frequency (62, 63). *lin-61* mutants also have defects in DNA repair (62, 63). A previous study reported that an *hpl-2(tm1489)* null mutant strain was hypersensitive to ionizing radiation (IR) (64); however, we found that this strain also harboured a deletion in the *polq-1* gene, which encodes DNA polymerase theta. Because *polq-1* mutants are reported to have increased sensitivity to DNA damaging agents and display genome instability (65), it was unclear if the defects observed were due to *hpl-2* (see Methods).

To determine whether *hpl-2* has a role in DNA repair, we tested the response of the isolated *hpl-2(tm1489)* mutant to IR induced DNA damage. Following IR, we observed that *hpl-2* mutants show higher levels of oocyte fragmentation compared to wild type, suggesting that they are defective in DNA repair (Figure 5-figure supplement 1). Additionally, *hpl-2* mutant germ lines are hypersensitive to induction of phosphorylation of the DNA damage checkpoint kinase CHK-1 (Figure 5-figure supplement 1). The hypersensitivity of *hpl-2* and *lin-61* mutants to exogenous DNA damage are consistent with increased genotoxic stress in the germ line.

We considered that the repeat desilencing and DNA repair defects of heterochromatin mutants might lead to increased germ line apoptosis, and thereby contribute to germ line and fertility defects. In wild-type animals, physiological

apoptosis occurs in the pachytene region of the gonad, with around half of the initially produced germ cells eliminated by apoptosis as a quality control mechanism (66). DNA damage causes increased apoptosis over physiological levels, and this increase is dependent on *cep-1*/p53 (67, 68). To assess germ line cell death in the heterochromatin mutants we used a CED-1::GFP reporter, which allows visualization of apoptotic germ cells in adult animals (69). We observed that *hpl-2, lin-13, lin-61*, and *set-25 met-2* mutants all displayed increased germ line apoptosis (Figure 5; *let-418* was not assayed because the apoptosis reporter used is genetically linked). Thus, heterochromatin factor mutants have increased germ cell death.

p53 is important for transduction of the DNA damage response and other stresses, and *C. elegans cep-1*/p53 is required for damage induced cell death (67, 68). We used RNAi to test whether activation of p53 dependent pathways played a role in heterochromatin mutant sterility. Following RNAi of *cep-1*/p53, we found that the brood sizes of *hpl-2, lin-13*, and *let-418* mutants grown at 25°C were modestly increased (Figure 4A). We further tested the effect of loss of *cep-1* by making double mutants with *cep-1(lg12501)*. Similar to the RNAi results, we observed that mutation of *cep-1* increased the fertility of *lin-13, let-418* and *hpl-2* mutants (Figure 4B). This increase is not due to a general effect of *cep-1* on fertility, as *cep-1* mutants have a slightly reduced brood size compared to wild-type animals (Figure 4B). We also observed that *cep-1* loss partially rescued the slow growth phenotype of the mutants (Figure 4C). These results suggest that genotoxic stress and DNA damage signalling in heterochromatin mutants activates p53, which contributes to sterility and slow growth. The increase in fertility upon *cep-1*/p53 inhibition may be a direct consequence of reduced germ line apoptosis, or alternatively the effect may be indirect, by preventing DNA damage signalling or improving growth rate. We also

note that although fertility of heterochromatin mutants is increased when *cep-1*/p53 is inhibited, it is not restored to wild-type levels indicating that other mechanisms contribute to sterility.

SPO-11 induced endogenous DNA damage contributes to heterochromatin mutant sterility

We next investigated whether endogenous physiological DNA damage may also contribute to heterochromatin mutant sterility. During meiosis, double strand breaks are induced by the topoisomerase-like protein SPO-11 to facilitate crossover formation and meiotic recombination (70). Similar to inhibition of damage induced cell death or MIRAGE1 expression, we found that inhibiting meiotic double strand breaks by RNAi of *spo-11* increased the brood size of *hpl-2, lin-13,* and *let-418* mutants (Figure 4A), suggesting that defects in repair of meiotic double strand breaks contributes to sterility.

The piRNA pathway shows similarity in repeat regulation and functional connections to heterochromatin factors

The piRNA pathway has a well-known role in preventing the activity of transposons in the germ line (34). In *C. elegans*, the piRNA pathway operates through the Piwi Argonaut protein PRG-1. Silencing occurs both transcriptionally, through engagement of the nuclear RNAi pathway, and post-transcriptionally, through a poorly understood mechanism. Interestingly, *prg-1* mutants have fertility defects, displaying a low brood size and a mortal germline phenotype that is more pronounced

356 at elevated temperatures (37, 38). The observation that heterochromatin mutants
357 desilence repetitive elements together with the finding that HPL-2 and H3K9
358 methyltransferse SET-25 are needed for piRNA pathway function in conjunction with
359 the nuclear RNAi pathway (35) prompted us to further investigate connections
360 between these factors.

361 We first assayed the expression of repetitive DNA in *prg-1* mutant adults
362 because genome-wide profiling had not previously been done. We detected
363 upregulation of 18 repetitive elements in *prg-1* mutants, 14 of which are also
364 upregulated in at least one of the heterochromatin mutants, including MIRAGE1
365 elements (Figure 6A, Figure 3-source data 1 and 2). RNA FISH experiments showed
366 that MIRAGE1 RNA is increased in *prg-1* mutant germ lines, similar to observations
367 in heterochromatin mutants described above (Figure 3E and Figure 3-figure
368 supplement 3). Given this overlap in targets and the fertility defects of *prg-1* mutants,
369 we assessed whether they also showed increased germ line apoptosis as seen in
370 heterochromatin factor mutants. Indeed, we observed significantly increased germ
371 cell death in *prg-1* mutant adults (Figure 6B). Therefore, the piRNA pathway and
372 heterochromatin factors have shared targets and phenotypes, and likely collaborate in
373 maintaining genomic integrity of the developing germline.

374 We next used a piRNA activity sensor to test whether heterochromatin factors
375 other than *hpl-2* are needed for piRNA pathway function. Similar to *hpl-2* and *set-25*,
376 we found that *lin-61* and *let-418* mutants derepress the piRNA sensor reporter (Figure
377 6C, D). We also observed weak desilencing in a fraction of *met-2* mutants (Figure 6D),
378 which was not observed in a previous assay (35). However, the piRNA sensor was
379 not desilenced in *lin-13* mutants. It is possible that the lack of desilencing is due to

the *lin-13(n770)* allele being non-null, however this mutant does show defects such as upregulation of repetitive elements and increased apoptosis.

A previous study profiling small RNAs in *hpl-2* mutants in a piRNA sensor background showed that piRNAs targeting the sensor or a few endogenous targets were not altered in abundance, suggesting that *hpl-2* acts downstream of piRNA production (35). To investigate this further, we compared the global abundance of piRNAs in *hpl-2* and wild-type adults. Similar to the above results, we found that *hpl-2* mutants make normal levels of piRNAs (Figure 6-figure supplement 1). We also investigated the production of secondary 22G siRNAs in *hpl-2* mutants. We detected a decrease in 22G RNAs mapping near predicted piRNA target sites in *prg-1* mutants as previously observed (41), but levels were normal in *hpl-2* mutants (Figure 6-figure supplement 1). *hpl-2* mutants also showed normal levels of 22Gs at repeat elements. (Figure 6-figure supplement 1). Therefore, at least for *hpl-2*, the role in the piRNA pathway appears to be downstream of piRNA and subsequent 22G RNA synthesis.

To summarize, *hpl-2*, *lin-61*, *let-418*, *set-25*, and *met-2* are important for piRNA pathway function. Nevertheless, the widespread binding sites and desilencing of additional targets relative to *prg-1* indicate that heterochromatin proteins also mediate repression that is not piRNA-induced.

Partial redundancy between *let-418*/Mi-2 and the nuclear RNAi pathway

The *C. elegans* nuclear RNAi pathway (called the nrde pathway) mediates transcriptional repression and directs H3K9me3 methylation to its targets (42, 44-47, 50). The nrde pathway also functions in repression of piRNA targets (35). To

investigate the relationship between the nrde pathway, the piRNA pathway, and heterochromatin factors in repetitive element regulation, we carried out RNA-seq on *nrde-2(gg91)*, a putative null mutant, and compared results to those of heterochromatin and *prg-1* mutants. We observed that *nrde-2* mutants showed a larger and different spectrum of repetitive element desilencing compared to *prg-1* or any of the heterochromatin mutants (Figure 7-figure supplement 1, Figure 3-source data 1 and 2). Of 71 elements desilenced in *nrde-2* mutants, only seven overlap a repeat desilenced in one of the heterochromatin mutant strains (Figure 7-figure supplement 1). Notably MIRAGE1 elements, prominently upregulated in heterochromatin and *prg-1* mutants, are not desilenced in *nrde-2* mutants (Figure 3-source data 1 and 2; Figure 7-figure supplement 1). Retrotransposons are highly enriched among *nrde-2* targets (45/71) whereas heterochromatin factors and *prg-1* are more associated with DNA transposon misregulation (Figure 3B). Therefore, although the nrde pathway is required for aspects of piRNA function, repetitive element targets largely differ. Notably, the finding that elements derepressed in *nrde-2* mutants differ from those in *met-2 set-25* mutants, which lack detectable H3K9 methylation, suggests that H3K9 methylation may not be required for nrde dependent repression.

Like the heterochromatin factor and *prg-1* mutants, *nrde-2* mutants also show a temperature sensitive decrease in fertility (42). To test whether the *nrde-2* fertility function had functional overlap with heterochromatin factors, we constructed double mutants between *nrde-2* and three mutants (*hpl-2, lin-61*, and *let-418*). We observed no reduction in fertility for *nrde-2; hpl-2*, and a weak but non-significant reduction for *nrde-2;lin-61* double mutants (Figure 7A). However, *nrde-2; let-418*, double mutants showed a significantly smaller brood size than expected compared to the single mutants, indicating partial functional redundancy between *let-418* and the nrde

pathway (Figure 7A). We also observed that all three double mutants showed significantly increased embryo lethality compared to the single mutants (Figure 7B).

To further investigate the genetic interaction between *nrde-2* and *let-418*, we carried out RNA-seq of *nrde-2; let-418* adults to test for redundancy in repeat element repression. We found that more repeats are upregulated in *nrde-2; let-418* double mutants compared to *nrde-2* or *let-418* single mutants (Figure 7B). Most of the repeat elements upregulated only in the *nrde-2; let-418* double mutant are retrotransposons (27/46; Figure 7B and Figure 3-source data 2). We conclude that NRDE-2 and LET-418 have unique and redundant roles in the repression of repetitive DNA elements.

Because a key output of the nrde pathway is the deposition of H3K9me3, the observed redundancy between NRDE-2 and LET-418 prompted us to investigate whether the nrde pathway might control H3K9me3 levels at heterochromatin regulated loci. To this end, we used published H3K9me3 ChIP-seq datasets in four different nrde mutants (*hrde-1, nrde-2*, *nrde-3*, and *nrde-4*; 44, 47, 51). and analysed levels at genes and repeats upregulated in *nrde-2* mutants or only in heterochromatin mutants. The nrde pathway acts in the germ line and soma: HRDE-1 and NRDE-3 are argonautes specific for germ line or soma, respectively, whereas NRDE-2 and NRDE-4 act in all tissues (42, 46, 47, 50). We observed that repeat elements and genes upregulated in *nrde-2* mutants also have reduced H3K9me3 levels, supporting the link between H3K9me3 methylation and repression of endogenous targets (Figure 7-figure supplements 2 and 3). H3K9me3 was also reduced on *nrde-2* upregulated elements in mutants of other nrde genes that act in the germ line (*hrde-1* and *nrde-4*), but not in the soma specific argonaute mutant *nrde-3* (Figure 7-figure supplements 2 and 3). This suggests that the transcriptional upregulation observed in *nrde-2* mutants occurs largely in the germ line.

453 We next analysed H3K9me3 levels in sets of genes and repeats upregulated in
454 heterochromatin mutant strains but not in *nrde-2* mutants to ask if these elements
455 were also under nrde control. Indeed, genes upregulated in any of the five
456 heterochromatin factor mutant strains (*hpl-2, lin-13, let-418, lin-61*, *met-2 set-25*) but
457 not in *nrde-2* mutants also showed reduced H3K9me3 in germ line nrde mutants,
458 though the reduction was weaker than for *nrde-2* regulated genes (Figure 7-figure
459 supplement 3). Repeats upregulated only in heterochromatin factor mutants showed a
460 trend of reduced H3K9me3 (Figure 7-figure supplement 2). Therefore, the germ line
461 nuclear RNAi pathway partially controls H3K9me3 levels at loci regulated by
462 heterochromatin factors. Because these elements are not upregulated in *nrde-2*
463 mutants, this indicates that the observed reduction of H3K9me3 is not sufficient for
464 derepression and supports partial redundancy between the nrde pathway and
465 heterochromatin factors in repeat silencing.

466

Discussion

All animal genomes contain abundant repetitive elements, which are subject to silencing control. This study expands our knowledge of repetitive element silencing by showing that a diverse set of heterochromatin factors (HPL-2/HP1, LIN-61, LET-418/Mi-2, LIN-13, and MET-2) work together with the piRNA and nuclear RNAi pathways to silence repetitive elements such as DNA transposons and retrotransposons. The systematic analyses of multiple factors, most of which are conserved, uncovered a network of functional interactions between them. We suggest that the interactions we identify here are likely to be relevant to the control of repetitive elements in other animals.

All factors and pathways studied are individually important for germ line function, as evidenced by reduced fertility or sterility of single mutants, and all are individually necessary for repetitive element silencing. Importantly, functional redundancy among the factors and pathways demonstrates widespread safeguards for ensuring germ line health and fertility. Our results show that there are interacting and overlapping mechanisms of repeat element silencing (Figure 8A).

Heterochromatin factors and small RNA pathways

Connections between heterochromatin formation and transcriptional silencing via RNAi mechanisms involving small RNAs have been observed in a variety of organisms (71, 72). For instance, RNAi machinery directs silencing at repetitive centromeric regions in *S. pombe* in a process that involves H3K9 methylation and chromodomain proteins that are similar to HP1. Likewise, in Arabidopsis and other

eukaryotes, repetitive elements have been shown to be repressed in chromatin by the action of nuclear pathways involving small RNAs and the targeting of H3K9 methylation. These pathways have also been implicated in gene silencing. However the mechanisms linking these silencing pathways are not fully understood and it is clear that factors involved in heterochromatin formation and function remain to be identified. For example a recent study of HP1a interactors in Drosophila identified many new factors needed for gene silencing and/or heterochromatin organization (73)

Previous studies in *C. elegans* have also uncovered connections between heterochromatin factors and small RNA pathways. The piRNA pathway is a small RNA pathway active in the germ line that silences transposons and genes through cytoplasmic and nuclear mechanisms (34). In the nucleus, the piRNA pathway engages the nrde pathway and heterochromatin factors for transcriptional repression: HPL-2, the H3K9me3 histone methyltransferase SET-25, and nuclear RNAi factors are necessary for silencing a piRNA pathway sensor (35). The nrde pathway directs H3K9me3 both endogenously and in response to exogenous dsRNA and effects transcriptional repression in both the germ line and soma (42, 44, 46, 50). Endogenous germ line nrde targets have been suggested to include retrotransposons based on their enrichment at genomic intervals with increased expression and decreased H3K9me3 levels in germ line nuclear RNAi mutants (51). Here, through genetic and profiling analyses, we have established additional connections between heterochromatin factors and small RNA pathways, linking them to repetitive element repression, uncovering functional redundancy, and expanding understanding of their relationships.

Heterochromatin factors associate with and repress repetitive elements

We found that the genome-wide distributions of each of the five heterochromatin factors studied here (HPL-2/HP1, LIN-13, LIN-61, LET-418/Mi-2, and MET-2/SETDB1) are highly correlated with each other and strongly associated with repetitive elements. These patterns are correlated with H3K9me2, but not with H3K9me3, as previously seen for HPL-2 in embryos (14). H3K9me2 and H3K9me3 modifications largely do not overlap (this study and (2)), but both are associated with repetitive elements. We further found that H3K9me2, but not H3K9me3 is enriched at telomeres. These patterns support functional differences between H3K9me2 and H3K9me3.

In addition to the similarity in binding profiles, we found that *hpl-2, lin-13, lin-61, let-418,* and *met-2 set-25* mutant strains all showed derepression of repetitive elements and genes. While this paper was under review, Zeller et al reported that *met-2 set-25* mutants derepressed transposable element expression in embryos and gonads, similar to the results presented here for *met-2 set-25* young adults (74). The global loss of H3K9 methylation also leads to transposon derepression and mobilization in Drosophila (75). The patterns of upregulated repetitive elements and genes among the five heterochromatin mutant strains are strikingly similar, indicating shared targets. However, although binding profiles and consequences of loss are similar, the factors also have unique roles. Furthermore, genetic interactions between all pairs show that they have partially redundant functions. To understand these relationships, it will be important to investigate their interdependencies and the consequences of inactivating multiple factors together.

Relationships between heterochromatin factors and small RNA pathways

539 Comparing expression profiles of heterochromatin mutants to those of *prg-1* (piRNA
540 pathway) and *nrde-2* (nuclear RNAi pathway) mutants, we observed that repeat
541 elements and genes have similar patterns of derepression in heterochromatin factor
542 and *prg-1* mutants, but these largely differ from those in *nrde-2* mutants. Consistent
543 with a functional link between the heterochromatin factors and the piRNA pathway, a
544 previous study showed that HPL-2 and SET-25 are needed for piRNA pathway
545 function (35). Here we further found that LIN-61, LET-418, and MET-2 (weakly) are
546 also important. It appears that heterochromatin proteins act as downstream effectors
547 of the piRNA pathway rather than having a role in small RNA biogenesis or stability
548 since levels of piRNAs and their secondary 22G RNAs are normal in *hpl-2* mutants
549 (35) (and this study). Investigating whether small RNA populations are altered in
550 other heterochromatin mutants will be needed to confirm this hypothesis. This
551 mechanism appears to differ from the situation in *S. pombe*, where H3K9 methylation
552 and chromodomain proteins are required for association of silencing complexes that
553 generate siRNAs (72, 76, 77). However, it is possible that redundancy between
554 heterochromatin factors in *C. elegans* may have masked involvement in small RNA
555 production.

556 Many more elements are desilenced in *nrde-2* mutants than in *prg-1* mutants,
557 with little overlap between the two. The elements derepressed in *nrde-2* mutants are
558 mostly LTR retrotransposons, in line with a study finding transcriptionally
559 upregulated genomic intervals in *hrde*-1 mutants to be enriched for LTRs and
560 unaffected in *prg-1* mutants (51). The apparent difference in targets between NRDE-
561 2 and PRG-1 could be due to the requirement for PRG-1 in initiation but not
562 maintenance of silencing. Once silencing is established by PRG-1, nuclear RNAi
563 maintains silencing in a process termed RNAe that depends on continued generation

564 of secondary siRNAs by mutator proteins, the presence of secondary siRNA-
565 associated argonautes (including *nrde-2*), and maintenance of the established
566 chromatin state by heterochromatin factors (35, 39-41, 78).

567 Our study also uncovered interactions between heterochromatin factors and
568 the nuclear RNAi pathway. We found that *let-418; nrde-2* double mutants show a
569 strongly enhanced fertility defect compared to the single mutants, and that they
570 desilence a larger set and a wider spectrum of repetitive elements. Therefore, for some
571 elements, either LET-418 or NRDE-2 is sufficient for silencing, demonstrating
572 redundancy in repetitive element silencing. These interactions further emphasize the
573 overlapping safeguards that function to effectively repress repetitive elements. The
574 increased embryo lethality seen in double mutants between *nrde-2* and three tested
575 heterochromatin factors (*hpl-2, lin-61*, or *let-418*) suggest additional as yet
576 unexplored redundancy between the nuclear RNAi pathway and heterochromatin
577 factors. That a substantial number of repetitive elements are desilenced in
578 heterochromatin factor mutants but not in *prg-1* or *nrde-2* mutants suggests that
579 heterochromatin factors can also act as independent agents, silencing repetitive
580 elements independently of small RNA pathways.

581 Interestingly, genes and repeats upregulated in *nrde-2* mutants more often
582 have high levels of H3K9me3 than H3K9me2 whereas those upregulated in *met-2 set-*
583 *25* mutants (which lack all H3K9 methylation) show the opposite pattern and more
584 often have high H3K9me2 marking (Figure 3-figure supplement 2). The association
585 between H3K9me3 and *nrde-2* upregulated genes suggests that the nuclear RNAi
586 pathway may specifically engage this modification. Consistent with this, repeats and
587 genes upregulated in *nrde-2* mutants have strongly reduced H3K9me3 levels in germ
588 line nuclear RNAi pathway mutants. However, the difference in elements desilenced

589 in *nrde-2* and *met-2 set-25* mutants (which lack H3K9 methylation) argues against an
590 essential requirement for H3K9 methylation in nrde mediated repression. We
591 observed that H3K9me3 levels in *nrde-2* and other germline nuclear RNAi mutants
592 are also weakly reduced at genes and repeats repressed by heterochromatin pathway
593 factors, even though these elements are not upregulated in *nrde-2* mutants. This
594 suggests that the heterochromatin factors and the nuclear RNAi pathway may regulate
595 many common elements, but that heterochromatin factors can still effectively silence
596 them in the absence of the nuclear RNAi pathway. Future analyses in mutants
597 compromised for both nuclear RNAi and heterochromatin factors will be needed to
598 address the mechanisms of this redundancy.

599

600 **Heterochromatin factors may act locally within euchromatic domains**

601 We speculate that in many cases, repetitive element regulation involves a local
602 mechanism rather than the spreading of large heterochromatin domains. First, we
603 observe that heterochromatin factor binding is often closely associated with repetitive
604 elements and does not extend to adjacent genes. Second, genes containing repetitive
605 elements bound by heterochromatin factors (usually within introns) are often
606 expressed. Indeed, one fourth of genes contain a repetitive element bound by a
607 heterochromatin factor, and of those, 59% (3287/5568) are expressed in the germ line.
608 Formation of a large inactive heterochromatin domain would clearly be incompatible
609 with such widespread germ line expression.

610 In *C. elegans*, most H3K9 marking occurs on the distal chromosome arms,
611 where small regions of H3K9 are interspersed with chromatin typical of euchromatin
612 (2). Many active genes, including those expressed in the germ line, reside in these

arm regions (2). Intriguingly, the repeat- and H3K9-rich chromosome arms are generally associated with the nuclear lamina, a region implicated in transcriptional repression (3, 79). Active genes at the periphery that contain repetitive elements bound by heterochromatin factors may be subject to special mechanisms for their expression.

Heterochromatin factors and DNA repair

In addition to functioning in repetitive element repression, some of the heterochromatin factors we studied here are implicated in DNA repair or genome stability. We found that *hpl-2* mutant germ lines show reduced repair and increased activation of DNA damage signaling in response to ionizing radiation. LIN-61 is needed for DNA repair in the germ line and its loss causes an increase in the germ line mutation rate (62, 63). Additionally, both *lin-61* and *set-25* were identified in a genome-wide RNAi screen for genes needed for genome stability in the soma (63). Furthermore, *met-2 set-25* mutants, which lack all H3K9methylation, were recently shown to have increased sensitivity to replication stress and increased rates of repeat associated mutations and R loops (74). In mammalian cells, orthologs of LET-418 (Mi-2), HPL-2 (HP1), and MET-2 (SETDB1), have documented roles in DNA repair (80-82). Mi-2 is needed for recruitment of DNA repair proteins to sites of DSBs, and loss of Mi-2 from human fibroblast cell lines leads to apoptosis and sensitivity to ionizing radiation (83-85). HP1 accumulates at DSBs and its depletion causes abnormal recruitment of repair factors (86). Additionally, DNA damage repair defects caused by depletion of SETDB1 are similar to those seen upon loss of HP1 (80). Defects in repair of DNA lesions are likely to cause germ line stress and to contribute

637 to the germ line instability, germ line development defects, and increased germ line
638 apoptosis seen in heterochromatin factor mutants. Such processes might also underlie
639 the reduced fertility and increased germ line apoptosis seen in *prg-1* mutants.

640 The activation of MIRAGE1 DNA transposases in all heterochromatin factor
641 mutant strains and *prg-1* mutants would be expected to cause double strand breaks
642 and/or replication stress. We show that this abnormal expression contributes to
643 sterility because fertility was partially restored in *hpl-2*, *let-418*, and *lin-13* mutants
644 when MIRAGE1 transcripts were knocked down via RNAi. Similarly, inhibiting
645 endogenous meiotic double strand breaks by knockdown of *spo-11* also partially
646 restored fertility. These results suggest that heterochromatin factors act to combat
647 different types of genotoxic insults, both through silencing repetitive elements and
648 facilitating repair. If not dealt with, these insults cause sterility (Figure 8B).

649 We also observed that loss of *cep-1*/p53 suppressed heterochromatin factor
650 defects. p53 is important for mediating DNA damage signaling (87). In *C. elegans*,
651 p53/*cep-1* is required for damage induced germ cell death (67, 68). In the soma, DNA
652 damage signaling does not lead to p53/CEP-1-mediated apoptosis; however, CEP-1
653 does play a role in DNA repair in the soma, and it slows larval development in
654 response to loss of CLK-2/TEL2 DNA damage signaling (88, 89). Our findings that
655 loss of *cep-1* partially suppresses the sterility and slow growth phenotypes of *hpl-2*,
656 *lin-13*, and *let-418* suggests that activation of damage signaling and *cep-1*/p53
657 underlies these defects.

658 Interestingly, none of the heterochromatin mutant strains studied here display
659 hallmarks of mutators such as high embryo lethality or the frequent production of
660 progeny with visible mutant phenotypes. We propose that quality control mechanisms

in the germ lines of heterochromatin factor mutants largely prevent improperly repaired meiotic germ cells from becoming mature gametes, either through apoptosis or the arrest of gametogenesis, to ensure that mutation rates are low.

Conclusions

This study indicates a complex orchestration of fertility protection by HPL-2/HP1, LIN-13, LIN-61, MET-2, and LET-418/Mi-2 together with the piRNA and nuclear RNAi pathways. Repression of repetitive elements may prevent replication stress and DNA damage, but when damage does occur, these heterochromatin proteins participate in repair pathways to maintain genome integrity. Further work will be required to untangle the mechanisms and individual roles in DNA repair pathways and repetitive element repression.

673 **Methods**

674 **Worm culture and strains**

675 Strains were cultured using standard methods (Brenner, 1974). Strains used in the
676 paper are given in Supplementary file 2. Whole genome sequencing of PFR40 *hpl-*
677 *2(tm1489)* identified an 882bp deletion in the *polq-1* gene at chrIII:5792238-5793119.
678 The underlined T residue marks the junction of the deletion and matches the flanking
679 sequence of both sides of the deletion:
680 TAAATCTCTATCCGATGTGATCCACGTCGATAACATTATTC; we have named
681 this lesion *polq-1(we100)*. The JA1902 strain harboring *hpl-2(tm1489)* but lacking
682 *polq-1(we100)* was derived by outcrossing MT15062 *hpl-2(tm1489);hpl-1(n4317)*,
683 which does not contain *polq-1(we100)*.

684

685 **ChIP-seq**

686 Wild-type young adults (YA) were prepared by growing synchronized L1s in liquid
687 culture using standard S-basal medium with HB101 E. coli for 60 hours at 20°C.
688 Adults were sucrose floated, washed in PBS, and flash frozen in liquid nitrogen.
689 Extract preparation and chromatin immunoprecipitation were performed as in (90)
690 with the following modifications: tissue was fixed for 10 minutes in 1.5 mM EGS
691 (Pierce 21565) then formaldehyde added to 1% for a further 10 minutes before
692 quenching with 0.125M glycine and washing 2X with PBS plus protease inhibitors.
693 Pellets were washed once in FA buffer, then resuspended in 1ml FA buffer per 1 mL
694 of ground worm powder and the extract sonicated to an average size of 250 base pairs
695 with a Diagenode Bioruptor or Bioruptor Pico for 28 pulses of 30 seconds followed

by 30 seconds pause. Antibodies used for ChIP are given in Supplementary file 3. Following ChIP and DNA purification, libraries were prepared using the Illumina TruSeq kit. Fragments in the 250-300 base pair range were selected using Agencourt AMPure XP beads. Two biological replicate ChIPs were conducted for each factor.

RNA-seq

Synchronized, starved L1 stage worms were grown on NGM plates at either 15°C (*lin-13*, *prg-1*, *nrde-2*, *nrde-2; let-418*, and N2) or 20°C (*hpl-2*, *let-418*, *lin-61*, *met-2 set-25*, and N2) until the L4 stage and then shifted to 25°C for 15-18 hours until they reached young adult stage. Worms were washed off plates at the young adult stage, flash frozen in liquid nitrogen, and stored at -80°C until use. RNA was extracted from frozen worms using TriPure (Roche). RNA was purified with Zymo Research RNA Clean and Concentrator-5 (Cambridge Bioscience) following DNAse I digestion. Ribosomal RNA was depleted using Ribo-Zero rRNA Removal Kit (Human/Mouse/Rat) (Illumina). Libraries were prepared using the NEBNext Ultra Directional RNA Library Prep Kit for Illumina (New England Biolabs). Two biological replicates were prepared for each strain.

Data Processing

ChIP-seq and RNA-seq libraries were sequenced using Illumina HiSeq. Reads were aligned to the WS220/ce10 assembly of the *C. elegans* genome using BWA v. 0.7.7 (91) with default settings (BWA-backtrack algorithm). The SAMtools v. 0.1.19 'view' utility was used to convert the alignments to BAM format. To be able to investigate

719 binding and expression at repetitive elements, we used all aligned reads (mapq0) to
720 generate pileup and normalised tracks. Normalized ChIP-seq coverage tracks were
721 generated using the BEADS algorithm (92) without the mappability correction step.
722 ChIP-seq and RNA-seq library read numbers and alignment statistics are given in
723 Figure 2-source data 3.

724

725 **Peak calls**

726 Broad and sharp ChIP-seq peaks were generated as follows. Initial ChIP-seq peaks
727 were called using MACS v. 2.1.1 (93) with a permissive 0.7 q-value cutoff and
728 fragment size of 150bp against a summed ChIP-seq input. These were used in
729 conjunction with a modified IDR procedure to generate broad peak calls ((94);
730 https://www.encodeproject.org/software/idr/) with an IDR threshold of 0.05 to
731 combine replicates. These broad peaks are termed “IDR peaks” (Figure 2-source data
732 1). The pipeline for generating IDR peaks is available here:
733 https://github.com/Przemol/biokludge/blob/master/macs2_idr/macs2_idr.ipy. To
734 generate sharp peak calls, the IDR calls were further refined using an adhoc post-
735 processing step, as visually distinct peaks close to each other were often contained
736 within single broad peaks. We identified concave regions within the IDR peaks using
737 the smoothed second derivative of the mapq0 pileup coverage signal with 250bp
738 kernel
739 (https://github.com/Przemol/biokludge/blob/master/macs2_idr/concave_regions.py).
740 We empirically found the minimum of the second derivative within a concave region
741 to be a good indicator of a visually compelling peak, and used concave regions
742 (within IDR peaks) with a threshold of lower than -500 curvature index. Next, we

743 discarded peaks with MASC2 score lower than 100 and peak width lower than 100bp.
744 The resulting peaks were filtered against combined ENCODE
745 (http://www.broadinstitute.org/~anshul/projects/worm/blacklist/ce10-blacklist.bed.gz)
746 and in-house blacklist
747 (https://gist.github.com/przemol/8a712a2e840f95237f4a4f322f65bee1) to generate
748 our final sharp peak calls, described as "concave peaks." We created a summary peak
749 call super set by creating a union of the five heterochromatin factor concave peak
750 calls. We termed this set "Any5" (n=33301; Figure 2-source data 1). Each Any5
751 region was then annotated for overlap with each factor. Venn diagrams were plotted
752 using VennDiagram R package (95), and UpSet plots were generated as described in
753 (96). For determination of factors bound to repeats, we used broad IDR peak calls
754 since repeats usually display a pattern of broad factor binding. Broad IDR peaks were
755 used in Figure 3-figure supplement 2.

756

757 **Differential expression analyses of genes**

758 We built an exon model based on Ensembl Gene 77 (Nov 2014) database gene
759 annotation lifted over to ce10/WS220. Tag counts for each gene were extracted from
760 BAM alignment files using HTSeq method working in union mode and implemented
761 in R. These values were used to build an expression matrix. Differential gene
762 expression between N2 and mutant backgrounds was tested using DESeq2; mutants
763 were compared to their temperature matched control N2 replicates (97). Reads per
764 kilobase of exon model per million mapped reads (RPKM) normalized expression
765 values were generated using the median ratio method (Equation 5 in Anders and
766 Huber, 2010). RPKM values, maximum posterior estimates of log2 FC (LFC) and

767 statistical significance estimates for each gene is in Figure 3-source data 3. We used a
768 false discovery rate (FDR) < 0.01 and LFC > 1 to call genes up-regulated, and FDR <
769 0.01 and LFC < -1 to call genes down-regulated. To avoid small differences in
770 developmental stages from contributing to apparent gene expression differences, we
771 also excluded genes whose wild-type expression oscillates repeatedly during
772 development (Supplemental Table S7 in(98)).

773

774 **Differential expression analyses of repeats**

775 We built a repeat element model based on Dfam 2.0 ((57), downloaded Sept 2015
776 from http://dfam.org/). The model contained 62331 individual repeats divided into
777 184 families. Since individual repeats did not had unique identifiers (UID), we named
778 them based on genomic position in "chromosome:start-end" convention, e.g.
779 "chrI:10773-11032". Tag counts for each repeat were extracted from BAM alignment
780 files using HTSeq method working in union mode and implemented in R. These
781 values were used to build expression matrixes. Differential repeat expression between
782 N2 and mutant backgrounds was tested using DESeq2 as described above for genes.
783 A table containing RPKM values, maximum posterior estimates of log2 FC (LFC)
784 and statistical significance estimates for each repeat is available in Figure 3-source
785 data 1. Upregulated repeats were defined as those with a false discovery rate (FDR) <
786 0.01, and LFC > 0. In addition, repeats that overlapped a gene upregulated in the
787 matched mutant background were filtered out. For purpose of filtering, differentially
788 expressed genes were defined with more permissive cutoffs: FDR < 0.05 and LFC >
789 0.

To assess expression of individual repeats scored as upregulated above, we counted uniquely mapping reads, defined as having a BWA mapping quality over 10. Elements with >10 unique reads and fold-change >1.5 were considered upregulated, which applied to 61 of 71 elements upregulated in any of the heterochromatin factor mutant strains. The remaining 10 elements had insufficient uniquely mapping reads for assessment.

Telomere enrichment

Telomere enrichment for ChIP-seq factors were determined by counting reads with the telomere sequence "GCCTAA". Reads were extracted from BAM files (including non- aligned reads) and trimmed to 36bp. Then the number of "GCCTAA" motifs was counted for each read using Biostrings R package. Telomeric reads were defined as those having 5 or 6 "GCCTAA" motifs in 36bp. To assess the statistical significance of enrichment we used one sided Mann–Whitney U test (2 replicates for each factor vs. input background of 129 experiments) and reported the p-values.

small RNA analyses

The following small RNA datasets from (35) were used: *prg-1* (GSM708661), WT matching *prg-1* (GSM708660), *hpl-2* (GSM950181), WT matching *hpl-2* (GSM950180), *nrde-2* (GSM950179), WT matching *nrde-2* (GSM950178). Uniquely matching positions in each dataset were determined and the smallest number (530039, in the *prg-1* dataset) subsampled from each. piRNA number was then determined by calculating the number matching the piRNAs annotated in (38) or (34) (n=27884

piRNAs). piRNA targets were determined as in (41), requiring a perfect match and no more than one G:U pair in the seed region (nt 2–8), and allowing up to two mismatches and an additional G:U pair outside of the seed region, excluding self hits (n=391173). piRNA dependent 22Gs were also defined as in (41), as 22G RNAs that mapped in 100bp windows centered at piRNA target sites, allowing zero or one mismatch.

H3K9me3 levels in nrde mutants

The following H3K9me3 ChIP seq datasets were used: *nrde-2* (GSM855086), *nrde-3* (GSM932875), *nrde-4* (GSM932876), WT for *nrde-2, -3, -4* (GSM855085), *hrde-1* (GSM1399632), and WT for *hrde-1* (GSM1399631) from (44, 47, 51). Datasets were processed as described in the data processing section above. The average signal in each region of interest was calculated and the H3K9me3 fold change was calculated relative to the matched wild-type dataset. Control repeats (n=612) have >1.5-fold H3K9me3 levels relative to the genome average, have <1-fold signal for each of the five heterochromatin factors (HPL-2, LIN-13, LIN-61, LET-418 and MET-2) relative to the genome average, and are not upregulated in any of the five mutant strains. A reduction of H3K9me3 at gene and repeat sets of interest was assessed by comparing to all genes or all repeats using a single-sided Mann-Whitney U test.

Detection of phospho-CHK-1

N2 and *hpl-2* adults grown at 25°C were irradiated at 0, 20, and 100 Gy and recovered for one hour at 25°C. One hour post irradiation, gonads were dissected in 8 µL M9 on slides and freeze-cracked. Gonads were fixed four minutes in 100 % methanol

837 followed by twenty minutes in 4 % formaldehyde in 1 X PBS. After fixation, gonads
838 were washed two times for ten minutes in 1 X PBS + 0.2 % Tween-20 (PBST),
839 blocked for one hour at room temperature in 1 % milk in PBST, washed two times for
840 ten minutes in PBST, incubated overnight at 4 °C in primary antibody diluted in
841 PBST (1:50 rabbit monoclonal α-phospho-CHK-1, Ser345, 133D, Cell Signalling
842 Technologies, catalogue #2348), washed two times for ten minutes in PBST,
843 incubated 2 hr with secondary antibody (Molecular Probes) and DAPI. Gonads were
844 scored for the presence of phospho-CHK-1 staining using a Zeiss 510 Meta scanning-
845 laser confocal microscope. Counts from individual experiments were pooled to give
846 overall totals, and a two-tailed proportions Z test was used to determine whether there
847 was a difference between N2 and *hpl-2* worms at a specific condition.

848

849 **Oocyte Chromatin Fragmentation Assay**

850 L4 N2 and *hpl-2(tm1489)* grown at 20°C were irradiated at 0, 50, and 100 Gy,
851 recovered for 24 hours at 20°C, then fixed in MeOH and DAPI stained. Slides were
852 scored for the number of DAPI bodies in diakinesis oocytes. Oocytes with six DAPI
853 bodies, representing the six bivalent chromosomes, were considered normal; oocytes
854 with other numbers of DAPI bodies, representing chromosome fracturing or clumping,
855 were considered fractured. To determine whether the proportion of oocytes with
856 fractured chromosomes was different between N2 and *hpl-2(tm1489)* worms at a
857 particular condition, a two-tailed proportions Z test was used. Two-tailed P values
858 were calculated using a Z score table.

859

860 **Germ line apoptosis measurements**

bcIs39 (Plim7::ced-1::GFP) expressed in gonadal sheath cells, was used to count engulfed germ line corpses (69). Strains containing *bcIs39* in wild type and mutant backgrounds were maintained at 20°C. L4s of each genotype were picked and 48 hours later scored for the number of engulfed apoptotic cells in the gonad. A minimum of 25 gonads per experiment were scored in three independent experiments. The number of apoptotic cells in the germ line observed with the *ced-1*::GFP is higher than the number stained by vital dye or visualized by Nomarski optics because the reporter also marks cells at earlier stages of apoptosis than can be detected by other methods (99, 100). In *lin-13*, *hpl-2*, and *met-2 set-25* strains, full or partial silencing of the GFP transgene reporter occurred in some individuals. These animals were excluded because it was not possible to count cell deaths. Statistical significance was scored using a Mann-Whitney non-parametric test over all the datapoints combined.

Assessment of abnormal oogenesis

Strains were maintained at 20°C and shifted to 25°C at the L4 stage. Adult germlines were imaged 48 hours later by mounting animals on 3% agarose pads in 5 mM Tetramisole, using a Zeiss widefield upright microscope using Nomarksi optics. Oogenesis was deemed 'abnormal' if oocytes appeared small and rounded, if they were disorganized, or if their cytoplasm had taken on a pronounced curdled texture. Germlines which had mostly or fully disintegrated, and lacked detectable oocytes, were also quantified.

Sterility interaction tests

884 Fertility interactions among heterochromatin factors were tested as follows: N2, *let-*
885 *418(n3536),* and *lin-13(n770)* were maintained at 20°C. Worms were fed at 20°C
886 from the L4 stage for the following RNAi clones from (101): *hpl-2* (K01G5.2), *met-2*
887 (R05D3.11), and *lin-61* (R06C7.7) or from starved L1s for *lin-13* (sjj2_C03B8.4).
888 RNAi plates were prepared as in (102). Progeny of fed L4s or the fed L1were singled
889 out onto fresh RNAi plates as L4s and total broods assessed by transferring the worms
890 to new plates every day until they stopped laying eggs. Two independent experiments
891 were conducted, with 3-8 total broods counted for each strain/RNAi combination.
892 Three double mutant combinations were also constructed and tested: *lin-61(tm2649);*
893 *lin-13(n770), lin-61(tm2649); hpl-2(tm1489),* and *hpl-2(tm1489); let-418(n3536).*
894 Wild-type N2, single mutants, and double mutant strains were maintained at 20°C and
895 total broods counted.

896 Fertility interactions between *nrde-2* and *let-418, hpl-2,* or *lin-61* were tested
897 as follows. Wild-type, single mutants, and double mutants were grown at 15°C from
898 starved L1 until the L3 stage, then transferred to 25°C. Total brood size per worm was
899 determined for 12-24 worms per strain across two independent experiments.
900 Genotypes of strains are given in Supplementary file 2.

901 Statistical tests for the above genetic interactions were conducted as follows:
902 Under the null hypothesis that the two genes do not interact to affect fertility, the
903 expected brood size of double mutant (or RNAi knockdown in a single mutant
904 background) is the product of those of the single mutants (or that of the single mutant
905 and the RNAi knockdown in a wild type background) divided by the brood size of the
906 wild-type (or of the wild-type strain grown on control (empty vector) RNAi plates).
907 Similar to (103), a t-test was used to test if the observed brood size of double mutants

908 (or RNAi knockdown in a single mutant background) equals the expected brood size
909 under the null hypothesis.

910 Tests for suppression of sterility of *hpl-2(tm1489)*, *lin-13(n770)*, and *let-*
911 *418(n3536)* mutants were conducted mutants as follows. The three strains show
912 temperature sensitive sterility. Strains were maintained at 20°C, a temperature at
913 which they are fertile, and starved L1s prepared by bleaching adults to collect
914 embryos and hatching them in M9 buffer for 24 hrs at 20°C. Starved L1s were
915 spotted onto RNAi plates prepared as in (102). They were then grown under
916 conditions at which the mutant strain is nearly sterile: *hpl-2* was incubated at 24°C or
917 25°C, *lin-13* was incubated at 24°C, and *let-418* was incubated for 7.5hrs at 20°C,
918 then shifted to 24°C. After three days, the number of progeny produced by these L1s
919 was counted. RNAi plates were prepared as in (102). The following RNAi clones
920 were from (101): *cep-1* (F52B5.5), *spo-11* (T05E11.4), *mirage-A* (K02E7.2 +
921 K02E7.3), *mirage-B* (W03G1.3 + W03G1.4). For each combination of mutant strain
922 and target gene to knockdown, a paired t-test was used to compare the average
923 number of progeny per parent from gene-targeting RNAi plates and matched empty
924 vector plates incubated under the same condition.

925 Brood sizes of *cep-1(lg12501); hpl-2(tm1489)*, *cep-1(lg12501);let-418(n3536)*
926 and *cep-1(lg12501);lin-13(n770)* double mutants were compared to wild-type and
927 single mutants. Adults raised at 15°C were bleached to obtain embryos and left at
928 20°C to hatch without food to obtain starved L1s. The starved L1s were fed with
929 OP50 bacteria and immediately shifted to 25°C (for *hpl-2* tests) or fed at 20°C for 7.5
930 hrs before shifting to 25°C (for *let-418* and *lin-13* tests). Experiments were repeated at
931 least twice and total brood sizes were determined for 8 to 40 worms per strain. L1s
932 prepared in the same way were used for growth rate tests, counting the number of

adults, L4s, or worms younger than L4 (indicated <L4) after approximately 48 hrs post feeding. A single sided t-test was used to test whether the brood size of the *cep-1* double mutant is larger than that of the single heterochromatin mutant.

piRNA sensor expression

mjIs144 [*mex*-5p::HIS-58::GFP::piRNA(21UR-1)::*tbb-2*-3'UTR] was used to assess piRNA pathway function (35). Synchronized larvae containing *mjIs144* in wild type or mutant backgrounds were maintained at 20°C, and scored for germ line expression 24 hours post-L4 stage. Four experiments were conducted per strain, with a minimum of 25 worms per experiment. GFP was scored using a Zeiss Axioplan 2 upright widefield microscope, where the level of GFP expression was assessed (none, low, moderate). Moderate expression was scored when GFP was easily detectible in oocytes and pachytene nuclei. Low expression was scored when GFP was just visible in oocyte and pachytene nuclei. In Figure 6, silenced represent gonads with no expression and Expressed - GFP(+) represent moderate or low expression. In the case of *met-2*, all expression was in the low category.

RNA FISH

N2, *hpl-2, lin-13, let-418, and prg-1* young adults were fixed and stained by RNA FISH as described (60). Stellaris® FISH probes targeting MIRAGE1 and *sqv-1* (as an internal control) were obtained from Bioresearch Technologies (Novato, CA). CAL Fluor Red610 was used for MIRAGE1 and Quasar 570 was used for *sqv-1*. From 11-22 individuals per strain were scored.

Datasets

Datasets generated in this paper are available at GEO accession GSE87524.

Acknowledgements

We are grateful to A. Akay for helpful comments on the manuscript. This work was supported by Wellcome Trust Senior Research Fellowships to JA (054523 and 101863). AM was supported by a fellowship from the Canadian Institutes of Health Research, DA by a Darwin Trust scholarship, and AS by an HFSP postdoctoral fellowship. EM was supported by grants from the Wellcome Trust (104640/Z/14/Z) and Cancer Research UK (C13474/A18583). JA and EM also acknowledge support by core funding from the Wellcome Trust (092096) and Cancer Research UK (C6946/A14492).

References

1. Wang J, Jia ST, & Jia S (2016) New Insights into the Regulation of Heterochromatin. *Trends in genetics : TIG* 32(5):284-294.
2. Liu T, *et al.* (2011) Broad chromosomal domains of histone modification patterns in C. elegans. *Genome research* 21(2):227-236.
3. Towbin BD, *et al.* (2012) Step-wise methylation of histone H3K9 positions heterochromatin at the nuclear periphery. *Cell* 150(5):934-947.
4. Zeng W, Ball AR, Jr., & Yokomori K (2010) HP1: heterochromatin binding proteins working the genome. *Epigenetics* 5(4):287-292.
5. James TC & Elgin SC (1986) Identification of a nonhistone chromosomal protein associated with heterochromatin in Drosophila melanogaster and its gene. *Molecular and cellular biology* 6(11):3862-3872.
6. Saksouk N, Simboeck E, & Dejardin J (2015) Constitutive heterochromatin formation and transcription in mammals. *Epigenetics & chromatin* 8:3.
7. Meier K & Brehm A (2014) Chromatin regulation: how complex does it get? *Epigenetics* 9(11):1485-1495.
8. Couteau F, Guerry F, Muller F, & Palladino F (2002) A heterochromatin protein 1 homologue in Caenorhabditis elegans acts in germline and vulval development. *EMBO reports* 3(3):235-241.
9. von Zelewsky T, *et al.* (2000) The C. elegans Mi-2 chromatin-remodelling proteins function in vulval cell fate determination. *Development* 127(24):5277-5284.
10. Melendez A & Greenwald I (2000) Caenorhabditis elegans lin-13, a member of the LIN-35 Rb class of genes involved in vulval development, encodes a protein with zinc fingers and an LXCXE motif. *Genetics* 155(3):1127-1137.
11. Schott S, Coustham V, Simonet T, Bedet C, & Palladino F (2006) Unique and redundant functions of C. elegans HP1 proteins in post-embryonic development. *Developmental biology* 298(1):176-187.
12. Koester-Eiserfunke N & Fischle W (2011) H3K9me2/3 binding of the MBT domain protein LIN-61 is essential for Caenorhabditis elegans vulva development. *PLoS genetics* 7(3):e1002017.
13. Wu X, Shi Z, Cui M, Han M, & Ruvkun G (2012) Repression of germline RNAi pathways in somatic cells by retinoblastoma pathway chromatin complexes. *PLoS genetics* 8(3):e1002542.
14. Garrigues JM, Sidoli S, Garcia BA, & Strome S (2015) Defining heterochromatin in C. elegans through genome-wide analysis of the heterochromatin protein 1 homolog HPL-2. *Genome research* 25(1):76-88.
15. Studencka M, *et al.* (2012) Transcriptional repression of Hox genes by C. elegans HP1/HPL and H1/HIS-24. *PLoS genetics* 8(9):e1002940.
16. Harrison MM, Lu X, & Horvitz HR (2007) LIN-61, one of two Caenorhabditis elegans malignant-brain-tumor-repeat-containing proteins, acts with the DRM and NuRD-like protein complexes in vulval development but not in certain other biological processes. *Genetics* 176(1):255-271.
17. Coustham V, *et al.* (2006) The C. elegans HP1 homologue HPL-2 and the LIN-13 zinc finger protein form a complex implicated in vulval development. *Developmental biology* 297(2):308-322.

18. Unhavaithaya Y, *et al.* (2002) MEP-1 and a homolog of the NURD complex component Mi-2 act together to maintain germline-soma distinctions in C. elegans. *Cell* 111(7):991-1002.
19. Passannante M, *et al.* (2010) Different Mi-2 complexes for various developmental functions in Caenorhabditis elegans. *PloS one* 5(10):e13681.
20. Andersen EC & Horvitz HR (2007) Two C. elegans histone methyltransferases repress lin-3 EGF transcription to inhibit vulval development. *Development* 134(16):2991-2999.
21. Kerr SC, Ruppersburg CC, Francis JW, & Katz DJ (2014) SPR-5 and MET-2 function cooperatively to reestablish an epigenetic ground state during passage through the germ line. *Proceedings of the National Academy of Sciences of the United States of America* 111(26):9509-9514.
22. Petrella LN, *et al.* (2011) synMuv B proteins antagonize germline fate in the intestine and ensure C. elegans survival. *Development* 138(6):1069-1079.
23. Poulin G, Dong Y, Fraser AG, Hopper NA, & Ahringer J (2005) Chromatin regulation and sumoylation in the inhibition of Ras-induced vulval development in Caenorhabditis elegans. *The EMBO journal* 24(14):2613-2623.
24. Simonet T, Dulermo R, Schott S, & Palladino F (2007) Antagonistic functions of SET-2/SET1 and HPL/HP1 proteins in C. elegans development. *Developmental biology* 312(1):367-383.
25. Yuan P, *et al.* (2009) Eset partners with Oct4 to restrict extraembryonic trophoblast lineage potential in embryonic stem cells. *Genes & development* 23(21):2507-2520.
26. Karimi MM, *et al.* (2011) DNA methylation and SETDB1/H3K9me3 regulate predominantly distinct sets of genes, retroelements, and chimeric transcripts in mESCs. *Cell stem cell* 8(6):676-687.
27. Bilodeau S, Kagey MH, Frampton GM, Rahl PB, & Young RA (2009) SetDB1 contributes to repression of genes encoding developmental regulators and maintenance of ES cell state. *Genes & development* 23(21):2484-2489.
28. Liu S, *et al.* (2014) Setdb1 is required for germline development and silencing of H3K9me3-marked endogenous retroviruses in primordial germ cells. *Genes & development* 28(18):2041-2055.
29. Maksakova IA, *et al.* (2013) Distinct roles of KAP1, HP1 and G9a/GLP in silencing of the two-cell-specific retrotransposon MERVL in mouse ES cells. *Epigenetics & chromatin* 6(1):15.
30. Greil F, *et al.* (2003) Distinct HP1 and Su(var)3-9 complexes bind to sets of developmentally coexpressed genes depending on chromosomal location. *Genes & development* 17(22):2825-2838.
31. de Wit E, Greil F, & van Steensel B (2005) Genome-wide HP1 binding in Drosophila: developmental plasticity and genomic targeting signals. *Genome research* 15(9):1265-1273.
32. Montoya-Durango DE, *et al.* (2016) LINE-1 silencing by retinoblastoma proteins is effected through the nucleosomal and remodeling deacetylase multiprotein complex. *BMC cancer* 16:38.
33. Hu G & Wade PA (2012) NuRD and pluripotency: a complex balancing act. *Cell stem cell* 10(5):497-503.

34. Weick EM & Miska EA (2014) piRNAs: from biogenesis to function. *Development* 141(18):3458-3471.
35. Ashe A, *et al.* (2012) piRNAs can trigger a multigenerational epigenetic memory in the germline of C. elegans. *Cell* 150(1):88-99.
36. Wang G & Reinke V (2008) A C. elegans Piwi, PRG-1, regulates 21U-RNAs during spermatogenesis. *Current biology : CB* 18(12):861-867.
37. Das PP, *et al.* (2008) Piwi and piRNAs act upstream of an endogenous siRNA pathway to suppress Tc3 transposon mobility in the Caenorhabditis elegans germline. *Molecular cell* 31(1):79-90.
38. Batista PJ, *et al.* (2008) PRG-1 and 21U-RNAs interact to form the piRNA complex required for fertility in C. elegans. *Molecular cell* 31(1):67-78.
39. Shirayama M, *et al.* (2012) piRNAs initiate an epigenetic memory of nonself RNA in the C. elegans germline. *Cell* 150(1):65-77.
40. Luteijn MJ, *et al.* (2012) Extremely stable Piwi-induced gene silencing in Caenorhabditis elegans. *The EMBO journal* 31(16):3422-3430.
41. Lee HC, *et al.* (2012) C. elegans piRNAs mediate the genome-wide surveillance of germline transcripts. *Cell* 150(1):78-87.
42. Guang S, *et al.* (2010) Small regulatory RNAs inhibit RNA polymerase II during the elongation phase of transcription. *Nature* 465(7301):1097-1101.
43. Gu W, *et al.* (2009) Distinct argonaute-mediated 22G-RNA pathways direct genome surveillance in the C. elegans germline. *Molecular cell* 36(2):231-244.
44. Gu SG, *et al.* (2012) Amplification of siRNA in Caenorhabditis elegans generates a transgenerational sequence-targeted histone H3 lysine 9 methylation footprint. *Nature genetics* 44(2):157-164.
45. Burton NO, Burkhart KB, & Kennedy S (2011) Nuclear RNAi maintains heritable gene silencing in Caenorhabditis elegans. *Proceedings of the National Academy of Sciences of the United States of America* 108(49):19683-19688.
46. Burkhart KB, *et al.* (2011) A pre-mRNA-associating factor links endogenous siRNAs to chromatin regulation. *PLoS genetics* 7(8):e1002249.
47. Buckley BA, *et al.* (2012) A nuclear Argonaute promotes multigenerational epigenetic inheritance and germline immortality. *Nature* 489(7416):447-451.
48. Mao H, *et al.* (2015) The Nrde Pathway Mediates Small-RNA-Directed Histone H3 Lysine 27 Trimethylation in Caenorhabditis elegans. *Current biology : CB* 25(18):2398-2403.
49. Allo M & Kornblihtt AR (2010) Gene silencing: small RNAs control RNA polymerase II elongation. *Current biology : CB* 20(17):R704-707.
50. Guang S, *et al.* (2008) An Argonaute transports siRNAs from the cytoplasm to the nucleus. *Science* 321(5888):537-541.
51. Ni JZ, Chen E, & Gu SG (2014) Complex coding of endogenous siRNA, transcriptional silencing and H3K9 methylation on native targets of germline nuclear RNAi in C. elegans. *BMC genomics* 15:1157.
52. Feng YL, Xiang JF, Kong N, Cai XJ, & Xie AY (2016) Buried territories: heterochromatic response to DNA double-strand breaks. *Acta biochimica et biophysica Sinica* 48(7):594-602.

53. Gursoy-Yuzugullu O, House N, & Price BD (2016) Patching Broken DNA: Nucleosome Dynamics and the Repair of DNA Breaks. *Journal of molecular biology* 428(9 Pt B):1846-1860.
54. Ceol CJ, Stegmeier F, Harrison MM, & Horvitz HR (2006) Identification and classification of genes that act antagonistically to let-60 Ras signaling in Caenorhabditis elegans vulval development. *Genetics* 173(2):709-726.
55. Thomas JH, Ceol CJ, Schwartz HT, & Horvitz HR (2003) New genes that interact with lin-35 Rb to negatively regulate the let-60 ras pathway in Caenorhabditis elegans. *Genetics* 164(1):135-151.
56. Sha K, *et al.* (2010) Distributed probing of chromatin structure in vivo reveals pervasive chromatin accessibility for expressed and non-expressed genes during tissue differentiation in C. elegans. *BMC genomics* 11:465.
57. Hubley R, *et al.* (2016) The Dfam database of repetitive DNA families. *Nucleic acids research* 44(D1):D81-89.
58. Chiolo I, *et al.* (2011) Double-strand breaks in heterochromatin move outside of a dynamic HP1a domain to complete recombinational repair. *Cell* 144(5):732-744.
59. Sinha M, Watanabe S, Johnson A, Moazed D, & Peterson CL (2009) Recombinational repair within heterochromatin requires ATP-dependent chromatin remodeling. *Cell* 138(6):1109-1121.
60. Raj A, van den Bogaard P, Rifkin SA, van Oudenaarden A, & Tyagi S (2008) Imaging individual mRNA molecules using multiple singly labeled probes. *Nature methods* 5(10):877-879.
61. Wallace NA, *et al.* (2013) HPV 5 and 8 E6 expression reduces ATM protein levels and attenuates LINE-1 retrotransposition. *Virology* 443(1):69-79.
62. Johnson NM, Lemmens BB, & Tijsterman M (2013) A role for the malignant brain tumour (MBT) domain protein LIN-61 in DNA double-strand break repair by homologous recombination. *PLoS genetics* 9(3):e1003339.
63. Pothof J, *et al.* (2003) Identification of genes that protect the C. elegans genome against mutations by genome-wide RNAi. *Genes & development* 17(4):443-448.
64. Luijsterburg MS, *et al.* (2009) Heterochromatin protein 1 is recruited to various types of DNA damage. *The Journal of cell biology* 185(4):577-586.
65. Muzzini DM, Plevani P, Boulton SJ, Cassata G, & Marini F (2008) Caenorhabditis elegans POLQ-1 and HEL-308 function in two distinct DNA interstrand cross-link repair pathways. *DNA repair* 7(6):941-950.
66. Gartner A, Boag PR, & Blackwell TK (2008) Germline survival and apoptosis. *WormBook : the online review of C. elegans biology*:1-20.
67. Schumacher B, Hofmann K, Boulton S, & Gartner A (2001) The C. elegans homolog of the p53 tumor suppressor is required for DNA damage-induced apoptosis. *Current biology : CB* 11(21):1722-1727.
68. Derry WB, Putzke AP, & Rothman JH (2001) Caenorhabditis elegans p53: role in apoptosis, meiosis, and stress resistance. *Science* 294(5542):591-595.
69. Zhou Z, Hartwieg E, & Horvitz HR (2001) CED-1 is a transmembrane receptor that mediates cell corpse engulfment in C. elegans. *Cell* 104(1):43-56.

70. Dernburg AF, *et al.* (1998) Meiotic recombination in C. elegans initiates by a conserved mechanism and is dispensable for homologous chromosome synapsis. *Cell* 94(3):387-398.
71. Castel SE & Martienssen RA (2013) RNA interference in the nucleus: roles for small RNAs in transcription, epigenetics and beyond. *Nature reviews. Genetics* 14(2):100-112.
72. Martienssen R & Moazed D (2015) RNAi and heterochromatin assembly. *Cold Spring Harbor perspectives in biology* 7(8):a019323.
73. Swenson JM, Colmenares SU, Strom AR, Costes SV, & Karpen GH (2016) The composition and organization of Drosophila heterochromatin are heterogeneous and dynamic. *eLife* 5.
74. Zeller P, *et al.* (2016) Histone H3K9 methylation is dispensable for Caenorhabditis elegans development but suppresses RNA:DNA hybrid-associated repeat instability. *Nature genetics* 48(11):1385-1395.
75. Penke TJ, McKay DJ, Strahl BD, Matera AG, & Duronio RJ (2016) Direct interrogation of the role of H3K9 in metazoan heterochromatin function. *Genes & development* 30(16):1866-1880.
76. Motamedi MR, *et al.* (2004) Two RNAi complexes, RITS and RDRC, physically interact and localize to noncoding centromeric RNAs. *Cell* 119(6):789-802.
77. Verdel A, *et al.* (2004) RNAi-mediated targeting of heterochromatin by the RITS complex. *Science* 303(5658):672-676.
78. de Albuquerque BF, Placentino M, & Ketting RF (2015) Maternal piRNAs Are Essential for Germline Development following De Novo Establishment of Endo-siRNAs in Caenorhabditis elegans. *Developmental cell* 34(4):448-456.
79. Ikegami K, Egelhofer TA, Strome S, & Lieb JD (2010) Caenorhabditis elegans chromosome arms are anchored to the nuclear membrane via discontinuous association with LEM-2. *Genome biology* 11(12):R120.
80. Alagoz M, *et al.* (2015) SETDB1, HP1 and SUV39 promote repositioning of 53BP1 to extend resection during homologous recombination in G2 cells. *Nucleic acids research* 43(16):7931-7944.
81. Polo SE, Kaidi A, Baskcomb L, Galanty Y, & Jackson SP (2010) Regulation of DNA-damage responses and cell-cycle progression by the chromatin remodelling factor CHD4. *The EMBO journal* 29(18):3130-3139.
82. Urquhart AJ, Gatei M, Richard DJ, & Khanna KK (2011) ATM mediated phosphorylation of CHD4 contributes to genome maintenance. *Genome integrity* 2(1):1.
83. Larsen DH, *et al.* (2010) The chromatin-remodeling factor CHD4 coordinates signaling and repair after DNA damage. *The Journal of cell biology* 190(5):731-740.
84. Pan MR, *et al.* (2012) Chromodomain helicase DNA-binding protein 4 (CHD4) regulates homologous recombination DNA repair, and its deficiency sensitizes cells to poly(ADP-ribose) polymerase (PARP) inhibitor treatment. *The Journal of biological chemistry* 287(9):6764-6772.
85. Smeenk G, *et al.* (2010) The NuRD chromatin-remodeling complex regulates signaling and repair of DNA damage. *The Journal of cell biology* 190(5):741-749.

86. Soria G & Almouzni G (2013) Differential contribution of HP1 proteins to DNA end resection and homology-directed repair. *Cell cycle* 12(3):422-429.
87. Meek DW (2009) Tumour suppression by p53: a role for the DNA damage response? *Nature reviews. Cancer* 9(10):714-723.
88. Derry WB, *et al.* (2007) Regulation of developmental rate and germ cell proliferation in Caenorhabditis elegans by the p53 gene network. *Cell death and differentiation* 14(4):662-670.
89. Hoffman S, Martin D, Melendez A, & Bargonetti J (2014) C. elegans CEP-1/p53 and BEC-1 are involved in DNA repair. *PloS one* 9(2):e88828.
90. Kolasinska-Zwierz P, *et al.* (2009) Differential chromatin marking of introns and expressed exons by H3K36me3. *Nature genetics* 41(3):376-381.
91. Li H & Durbin R (2010) Fast and accurate long-read alignment with Burrows-Wheeler transform. *Bioinformatics* 26(5):589-595.
92. Cheung MS, Down TA, Latorre I, & Ahringer J (2011) Systematic bias in high-throughput sequencing data and its correction by BEADS. *Nucleic acids research* 39(15):e103.
93. Feng J, Liu T, Qin B, Zhang Y, & Liu XS (2012) Identifying ChIP-seq enrichment using MACS. *Nature protocols* 7(9):1728-1740.
94. Li Q, Brown, J.B, Huang, H., and Bickel, P.J. (2011) Measuring reproducibility of high-throughput experiments. *Ann. Appl. Stat.* 5:1752-1779.
95. Chen H & Boutros PC (2011) VennDiagram: a package for the generation of highly-customizable Venn and Euler diagrams in R. *BMC bioinformatics* 12:35.
96. Lex A, Gehlenborg N, Strobelt H, Vuillemot R, & Pfister H (2014) UpSet: Visualization of Intersecting Sets. *IEEE transactions on visualization and computer graphics* 20(12):1983-1992.
97. Love MI, Huber W, & Anders S (2014) Moderated estimation of fold change and dispersion for RNA-seq data with DESeq2. *Genome biology* 15(12):550.
98. Latorre I, *et al.* (2015) The DREAM complex promotes gene body H2A.Z for target repression. *Genes & development* 29(5):495-500.
99. Lant B & Derry WB (2014) Fluorescent visualization of germline apoptosis in living Caenorhabditis elegans. *Cold Spring Harbor protocols* 2014(4):420-427.
100. Lu N, Yu X, He X, & Zhou Z (2009) Detecting apoptotic cells and monitoring their clearance in the nematode Caenorhabditis elegans. *Methods in molecular biology* 559:357-370.
101. Kamath RS, *et al.* (2003) Systematic functional analysis of the Caenorhabditis elegans genome using RNAi. *Nature* 421(6920):231-237.
102. Ahringer (ed.) J (Reverse genetics. in *WormBook : the online review of C. elegans biology*, ed Community TCeR (Wormbook).
103. Baugh LR, *et al.* (2005) Synthetic lethal analysis of Caenorhabditis elegans posterior embryonic patterning genes identifies conserved genetic interactions. *Genome biology* 6(5):R45.

Figure legends

Figure 1. Heterochromatin proteins have redundant roles in fertility.

(A) Genetic interactions in fertility assayed using RNAi. Indicated RNAi of wild-type, *let-418(n3536)*, *or lin-13(n770)* was conducted by feeding at 20°C as described in the methods. Results are a combination of two independent experiments with the progeny of 3-8 total broods counted for each strain/RNAi combination. A one-sided t-test was used to determine whether the mutant/RNAi combination had a lower brood size than expected under a multiplicative model of interaction when compared to the mutant grown on empty vector RNAi and the individual RNAi knockdowns in wild-type animals. Brood size is significantly lower than expected for all RNAi/mutant combinations at $p<0.05$. (B) Indicated double mutants were constructed and their brood sizes compared to that of the individual signal mutants raised at 20°C. Statistical testing was as in (A), with brood sizes of the three double mutants significantly lower than expected at $p<0.05$ in a one-sided t-test. (C) All pairs of *hpl-2, lin-13, lin-61, let-418*, and *met-2* show genetic interactions in fertility, as determined in this study or previous studies. ref 1. Coustam et al, *Dev Biol.* 2006. ref 2. Koester-Eiserfunke and Fischle, *PLoS Genet.* 2011. ref 3. Simonet et al, *Dev Biol.* 2007. Supplementary file 1 shows previously reported sterility phenotypes. Figure 1 – figure supplement 1 shows examples and quantification of abnormal oogenesis in heterochromatin mutants.

Figure 2. HPL-2, LET-418, LIN-13, LIN-61, and MET-2 show extensive co-binding and are enriched at repetitive elements.

(A) Distribution of the indicated proteins and histone modifications over each *C. elegans* chromosome. z-scored ChIP-seq tracks are shown for HPL-2 (red), LET-418 (blue), LIN-13 (green), LIN-61 (orange), MET-2 (pink), H3K9me2 (grey) and H3K9me3 (black) on each chromosome, demonstrating enrichment over the autosomal arms. Figure 2-figure supplement 1A shows distributions of peak locations in different chromosome regions. (B) IGV browser screenshot showing similar patterns of the heterochromatin factors and H3K9me2 methylation over a 45 kb region containing multiple repeat elements. z-scored ChIP-seq tracks are as in (A). Any5 peak calls denote combined peak calls for any of the five proteins; repeats are from Dfam2.0 {Hubley, 2016 #4}. Figure 2-figure supplement 1B shows correlations in signal between all datasets. (C) UpSet plot of the association of heterochromatin factors with the 33,301 Any5 peak calls. Dots indicate peak class is bound by the factor. Bars show total number of peaks per class, the orange portion denoting overlap with repeat elements. Below the bar chart relative enrichments for H3K9me2 and H3K9me3 are shown. The peaks that overlap all 5 factors constitute the largest class (n=4810). Figure 2-figure supplement 1 gives total peak numbers per factor, number of peaks overlapping repeats, and number of repeats bound by each factor. Figure 2-source data 1 gives peak calls. (D) Associations of factors and repeat classes. Upper panel: levels of indicated protein or histone modification on families within indicated Dfam 2.0 repeat classes relative to the genome average. Bottom panel: Proportion of families within each repeat class significantly enriched for

indicated factor or histone modification. Criteria for enrichment are >1.5 fold mean enrichment of family relative to genome, FDR<0.1, considering families with at least 10 members. Number of families with 10 or more members within each class are: Cut and paste (n=89), Helitron (n=7), LTR (n=31), LINE (n=13), SINE (n=3), Satellite (n=16), Unknown (n=7). Figure 2-source data 2 gives enrichment scores for repeat family factor binding.

Figure 3. Repetitive elements are upregulated in *hpl-2, let-418, lin-13*, *lin-61*, *met-2 set-25, prg-1, nrde-2, and nrde-2; let-418* mutants.

(A) Venn diagram of elements upregulated in *hpl-2*, *let-418*, *lin-13*, *lin-61*, and *met-2 set-25* mutants. The seven elements upregulated in all five strains are MIRAGE1 elements. (B) Distribution of Dfam 2.0 repeat classes upregulated in each strain. (C) Repeat families with members upregulated in at least one of *hpl-2*, *let-418*, *lin-13*, *lin-61*, or *met-2 set-25* mutant strains. (D) IGV browser screenshot of a MIRAGE1 element that is upregulated in all mutant strains. Tracks are reads per million of two combined replicates. Figure 3-figure supplement 1 gives further examples of elements upregulated in different strains. (E) Single molecule RNA-FISH signals of MIRAGE 1 element RNA in the adult germ line (white dots). Signal is not detectable in wild-type but is abundant in the indicated mutant backgrounds. Figure 3 – figure supplement 3 shows additional images of MIRAGE1 and *sqv-1* control RNA FISH in germline and somatic tissues. Figure 3-figure supplement 2 shows enrichment of heterochromatin factors, H3K9me2, and H3K9me3 on regulated genes and repeats.

Figure 4. Phenotypic suppression of *hpl-2, let-418* and *lin-13* by inhibition of MIRAGE1, *cep-1/p53*, or *spo-11*

(A) RNAi of MIRAGE1, *cep-1*/p53 or *spo-11* partially suppresses sterility of *hpl-2, let-418*, and *lin-13*. Average number of progeny per worm for control empty vector RNAi (EV) or the indicated RNAi treatments in *hpl-2(tm1489)*, *let-418(n3536)*, or *lin-13(n770)* (averages of 5-11 experiments). Experiments were done under conditions where the mutant strain was nearly sterile to detect an increase in fertility (see Methods). Control progeny numbers vary by experiment, but were always paired with experimental RNAi. Stars indicate statistical significance assessed using paired t-tests, comparing experimental to control RNAi ($p<0.05$, one star; $p<0.01$, two stars; $p<0.001$, three stars). Two sets of RNAi clones were used to target MIRAGE1 elements (termed mirage-A and mirage-B). RNAi clones used are given in the methods. (B) Mutation of *cep-1*/p53 partially suppresses sterility of *hpl-2, let-418*, and *lin-13* mutants at 25°C. Statistical significance was assessed using single sided t-tests, asking if *cep-1; hpl-2*, *cep-1; let-418*, and *cep-1; lin-13* double mutants had larger broods than the corresponding heterochromatin single mutants. See methods for growth conditions. (C) Loss of *cep-1* partially rescues growth delay defect of heterochromatin mutants at 25°C. Developmental stage of worms grown from L1 at 25C for approximately 48 hrs was assessed (adult, L4, younger than L4). A

representative experiment out of three replicates is shown, assaying between 95 and 213 worms in each. See methods for growth conditions.

Figure 5. Heterochromatin mutants have increased germline apoptosis.

CED-1::GFP (*bcIs39* [P*lim-7::ced-1::gfp*]), expressed in gonad sheath cells, marks engulfed apoptotic cells in the pachytene region of the adult gonad. (A) CED-1::GFP images for wild type, *hpl-2*, and *met-2 set-25* mutant gonads. Arrows point to engulfed apoptotic cells; scale bar = 16 um. (B) Number of apoptotic cells per gonad arm for wild-type (*bcIs39*), *hpl-2(tm1489); bcIs39, lin-13(n770); bcIs39*, and *met-2(n4256) set-25(n5021); bcIs39*. Shown are the combined data points of at least 3 independent replicates; each dot represents an individual gonad arm count. Bars denote mean and SD. Mann-whitney non-parametric tests were performed on mutant versus control. (p-values for *hpl-2, lin-61, met-2 set-25* are <0.0001; p-value for *lin-13* is 0.009). Strains were cultured at 20°C and scored 48 hrs after the L4 stage. Figure 5 –figure supplement 1 shows increased sensitivity of *hpl-2* to IR-induced DNA damage.

Figure 6. Heterochromatin factors interact with the piRNA pathway.

(A) Venn diagram showing extent of overlap between repeats upregulated in *prg-1* mutants and repeats upregulated in any of the five heterochromatin factor mutant strains (*hpl-2, let-418, lin-13, lin-61*, or *met-2 set-25*). Listed in the Venn are the numbers of repeats and repeat families common or unique to *prg-1*. (B) *prg-1* mutant germ lines show increased germ cell death. Shown are the number of apoptotic cells per gonad arm for *bcIs39* (CED-1::GFP) and *prg-1; bcIs39* (CED-1::GFP). Each dot represents an individual gonad arm count. Bars denote mean and SD. A minimum of 25 gonads were scored per experiment and shown are the combined datapoints of at least 3 independent replicates. Mann-whitney non-parametric tests were performed on mutant versus control (P-value <0.0001). Strains were cultured at 20°C until L4 stage, then shifted to 25°C for 48 hrs before scoring. (C ,D) Heterochromatin mutants desilence a piRNA sensor. piRNA sensor expression (*mjIs144* [mex-5p::HIS-58::GFP::piRNA(21UR-1)::tbb-2-3'UTR]) was quantified in one day old wild-type and heterochromatin mutants cultured at 20°C. (C) Representative GFP and DIC microscope images of adult germlines in which the reporter is silent (WT, *lin-13)* or expressed (*lin-61*). (D) Quantification of piRNA sensor expression in wild type and heterochromatin mutants. Shown are the means and standard error of the percentage of worms which at least weakly desilenced the GFP reporter in oocytes and pachytene regions. A minimum of 100 worms for each strain was assessed over four independent experiments. Fishers exact tests were performed on the combined datapoints to address significance, with *let-418* (p-value <0.0001), *lin-61* (p-value <0.0001) and *set-25* (p-value <0.0001) all displaying increased frequency of expression of the piRNA sensor reporter, while sensor expression in *lin-13* is

not significantly different from wild type (p-value 0.4419). *met-2* mutants weakly desilence the sensor in a small subset of adults scored (p-value 0.0215).

Figure 7. *nrde-2* and *let-418* show functional redundancy.

(A) *nrde-2* and *let-418* mutants show genetic interaction in fertility. Brood sizes of *nrde-2; hpl-2, nrde-2; let-418*, and *nrde-2; lin-61* double mutants were compared to those of single mutants. Synchronized single or double mutant strains of the indicated genotype were grown at 15°C until the L3 stage and then transferred to 25°C, and total progeny including dead embryos determined for 12-24 mothers across two independent experiments. A single-sided Mann-Whitney U test was used to determine whether the double mutant had a lower brood size than expected under a multiplicative model of interaction when compared to the individual single mutants. Brood size is significantly lower than expected for *nrde-2; let-418* (p =9.21E-11) but not *lin-61; nrde-2* (p=0.20) or *nrde-2; hpl-2 (*p=98). (B) *nrde-2; hpl-2, nrde-2;let-418* and *lin-61;nrde-2* double mutants show increased proportion of dead embryos within their broods compared to single mutants. Total number of dead embryos was determined as a proportion relative to their total brood size for the experiment in (A). Mann-Whitney U tests were performed to compare the proportion of unhatched eggs in double mutants relative to *nrde-2* single mutants, and were all found to be significant at $p<0.05$. (C) Repeat families with members upregulated in *let-418*, *nrde-2*, and *nrde-2; let-418* young adult worms. Figure 7-figure supplement 1A compares repeat families upregulated in *nrde-2*, *prg-1*, or any of the five heterochromatin mutants (D) Example of repeats upregulated in *nrde-2; let-418*, but not the single mutants. Tracks are RNA-seq reads per million of two combined replicates. Figure 7-figure supplement 1B shows lack of MIRAGE1 expression in the *nrde-2* mutant background.

Figure 8. Heterochromatin proteins collaborate with small RNAi pathways to maintain fertility.

(A) Pathways of transposable element silencing in *C. elegans*. Heterochromatin factors participate in repetitive element silencing together with the piRNA and nuclear RNAi pathways, as well as targeting elements independently of these pathways. (B) Derepression of transposable elements and defects in DNA repair likely generate genotoxic stress that leads to germ line defects and infertility in heterochromatin factor mutants.

Legends for Figure Supplements:

Figure 1 – figure supplement 1. Heterochromatin mutants display abnormal oogenesis

(A) Strains of the indicated genotype were shifted to 25°C at the L4 stage and imaged by Nomarksi microscopy 48 hours later. Oocyte quality was determined and deemed 'abnormal' when oocytes appeared small, round and gapped, showing the appearance of a curdled cytoplasm, or when they were unaligned and disorganized. Numbers in brackets denote the total number of germlines scored. Disintegrated germline refers to the absence of oocytes and an apparent disintegration of (most of the) gonad arm. Representative images of several of the mutants are shown. Scale bar is 33 μm.

Figure 2-figure supplement 1. Correlation of HPL-2, LET-418, LIN-13, LIN-61, and MET-2 ChIP-seq tracks and enrichment on chromosome arms, repetitive elements, and telomeres.

(A) Distribution of HPL-2, LET-418, LIN-13, LIN-61, MET-2, All5, or Any5 ChIP-seq peaks between chromosome arms and centers (left) and between genes (introns and exons) and intergenic regions on the centers (middle) and arms (right). (B) Pearson correlation coefficients for ChIP-seq track combined replicates in 100 bp windows. (C) Number of peaks for individual data sets within the 33301 Any5 combined peak calls, the numbers unique to each dataset and the numbers of peaks overlapping repetitive elements. (D) Numbers of Dfam 2.0 repetitive elements (n = 62331) that have factors bound based on IDR peak calls (see Methods). (E) Enrichment scores for H3K9 methylation and binding of factors at telomeres.

Figure 3-figure supplement 1. Examples of unique and co-regulated repeat elements in various heterochromatin mutants.

IGV screenshots of repeat elements upregulated in a subset of heterochromatin mutants. (A) HELITRON1 element only upregulated in *lin-13* mutants. (B) PALTTAA2 and CELE46B elements only upregulated in *hpl-2* mutants. (C) CER16 LTR element upregulated in *hpl-2*, *lin-61, nrde-2* and *nrde-2; let-418* mutants. Signal tracks are RPM normalized. Additional tracks show genes, Dfam2.0 repeats, and transposon ORFs.

Figure 3-figure supplement 2. Heterochromatin factors and H3K9 methylation show enriched association with upregulated genes and repeats.

(A) Percent overlap of heterochromatin factor peaks or >1.5 fold enrichment for H3K9me2 or H3K9me3 on upregulated (left) or downregulated (right) genes (-

500 bp to gene end). Parentheses give number of genes with overlap, star indicates FDR<0.01. (B) Enrichment of factors over upregulated repeats in each of the mutant strains.

Figure 3-figure supplement 3. MIRAGE1 RNA is upregulated in the germ lines of *hpl-2, lin-13, let-418,* and *prg-1* mutants.

(A) Single molecule RNA-FISH signals of MIRAGE 1 RNA in the adult germ line (left panels; zoomed in on the right). Middle panels show *sqv-1* (positive control) RNA-FISH and DAPI to counterstain nuclei. (B) Single molecule RNA-FISH signals of MIRAGE 1 RNA, showing both germline and somatic tissues. MIRAGE1 (middle and indicated boxes zoomed in on the right) is increased in mutant germlines but remains low in the soma. Left, DAPI counterstain. Scale bar represents 30 μm.

Figure 5-figure supplement 1. *hpl-2* mutants are hypersensitive to ionizing radiation-induced DNA damage.

(A)Phospho-CHK-1 staining of adult germ lines 1 hr post IR treatment. Bars are 10 μm. (B) Quantification of phospho-CHK-1 staining. *hpl-2* mutants showed significantly more phospho-CHK-1 positive gonads than wild-type at an intermediate dose of 20 Gy. Strains were grown at 25°C. (C) Images and counts of oocyte chromosomes and fragments following IR. N2 and *hpl-2(tm1489)* were grown at 20°C, irradiated at 0, 50, and 100 Gy at the L4 stage, and stained with DAPI after 24 hours. Left, representative photographs of N2 and *hpl-2* oocytes. Right, counts of DAPI stained fragments in oocytes at the indicated dose of IR. The majority of non-irradiated N2 and *hpl-2* oocytes have 6 distinct DAPI bodies, representing the 6 bivalent chromosomes. *hpl-2* mutants show more fragmentation of oocyte chromosomes at 50 and 100 Gy, indicating a defect in repair of exogenous DNA damage. Bars are 5 μm. A minimum of 88 oocytes were scored over two to three independent experiments.

Figure 6-figure supplement 1. Quantification of piRNAs and dependent 22G RNAs in *prg-1* and *hpl-2* mutants

(A) Unique piRNAs, repeat elements targeted by a piRNA, number of unique 22G RNAs mapping near piRNA target sites, and number of repeat elements hit by a piRNA-associated 22G RNA. The number in each class found in 530039 unique small RNA positions subsampled from each dataset (*prg-1, hpl-2,* and matched wild-types) is shown. (B) log2 ratios of the relative change in abundance of the indicated classes of small RNA or repeats in mutant strains compared to wild-type. Datasets used and the procedure for calculating piRNA and dependent 22G RNA number is given in the Methods.

Figure 7-figure supplement 1. Overlap of *nrde-2, prg-1*, and heterochromatin targets.

(A) Repeat families with members upregulated in *nrde-2*, *prg-1*, and any of the five heterochromatin mutants (*let-418, hpl-2*, *lin-13*, *lin-61*, and *met-2 set-25*).

Families in bold are specific to a particular overlap. (B) RNA-seq tracks showing MIRAGE element upregulated in heterochromatin factor and *prg-1* mutants but not in *nrde-2* mutants.

Figure 7-figure supplement 2. H3K9me3 levels on repeats in nrde mutants

(Top) H3K9me3 log2FC of average signal at indicated regions in *hrde-1, nrde-2, nrde-4*, and *nrde-3* mutants relative to wild-type. Control repeats have >1.5 fold average signal in wild-type relative to genome average, and no enrichment for any heterochromatin factor. *nrde-2*, all repeats upregulated in *nrde-2* mutants; any5 Heterochromatin, repeats upregulated in any of the 5 heterochromatin mutant strains, but not in *nrde-2* mutants; *prg-1*, repeats upregulated in *prg-1* mutants but not in *nrde-2* mutants. Parentheses show number of elements in each set. A reduction of H3K9me3 at repeat sets of interest was assessed by comparing to all repeats using a single-sided Mann-Whitney U test: one star, $p<0.1$, two stars, $p<0.05$; three stars, $p<0.001$. (Bottom) H3K9me3 levels relative to genome average at indicated regions in each dataset.

Figure 7-figure supplement 2. H3K9me3 levels on genes in nrde mutants

(Top) H3K9me3 log2FC of average signal at indicated regions in *hrde-1, nrde-2, nrde-4*, and *nrde-3* mutants relative to wild-type. *nrde-2*, genes upregulated in *nrde-2* mutants. For each of the other strains, gene sets are those upregulated in the indicated mutant but not upregulated in *nrde-2* mutants. Parentheses show number of genes in each set. A reduction of H3K9me3 at gene sets of interest was assessed by comparing to all genes using a single-sided Mann-Whitney U test: one star, $p<0.1$, two stars, $p<0.05$; three stars, $p<0.001$. (Bottom) H3K9me3 levels relative to genome average at indicated regions in each dataset.

Supplementary files

Supplementary file 1. LET-418, LIN-13, HPL-2, LIN-61, and MET-2 are required for normal fertility.

Supplementary file 2. Strains used in this study.

Supplementary file 3. Antibodies used in this study.

Source data files

Figure 2-source data 1 - Peak calls

Figure 2-source data 2. Enrichment of factors at repeat families

Figure 2-source data 3 - Alignment Statistics for ChIP and RNA sequencing

Figure 3-source data 1 -Analysis of repeats

Figure 3-source data 2 - Repeats upregulated in any mutant strain

Figure 3-source data 3 - Analysis of genes

A

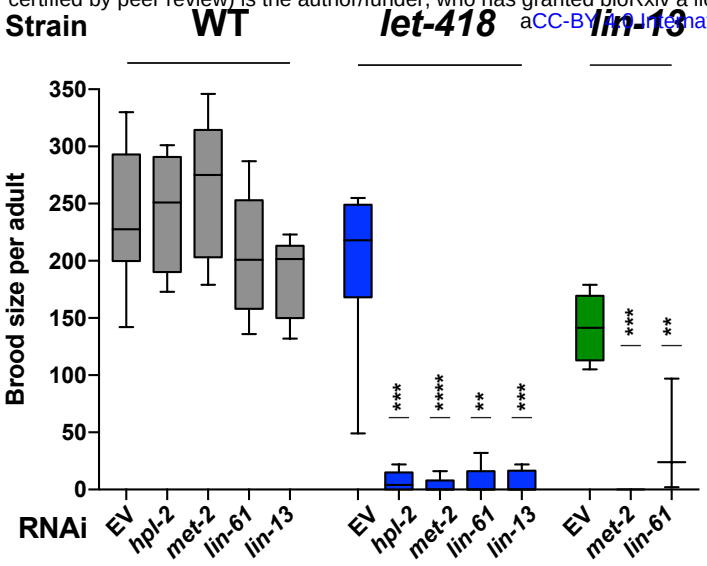

B

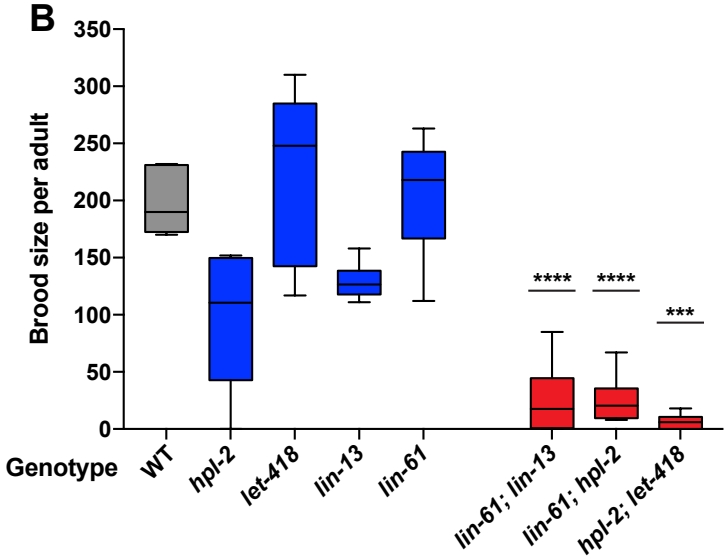

C

	hpl-2	*lin-13*	*lin-61*	*let-418*
lin-13	ref 1			
lin-61	ref 2	This study		
let-418	This study	This study	This study	
met-2	refs 2,3	This study	ref 2	This study

Figure 1

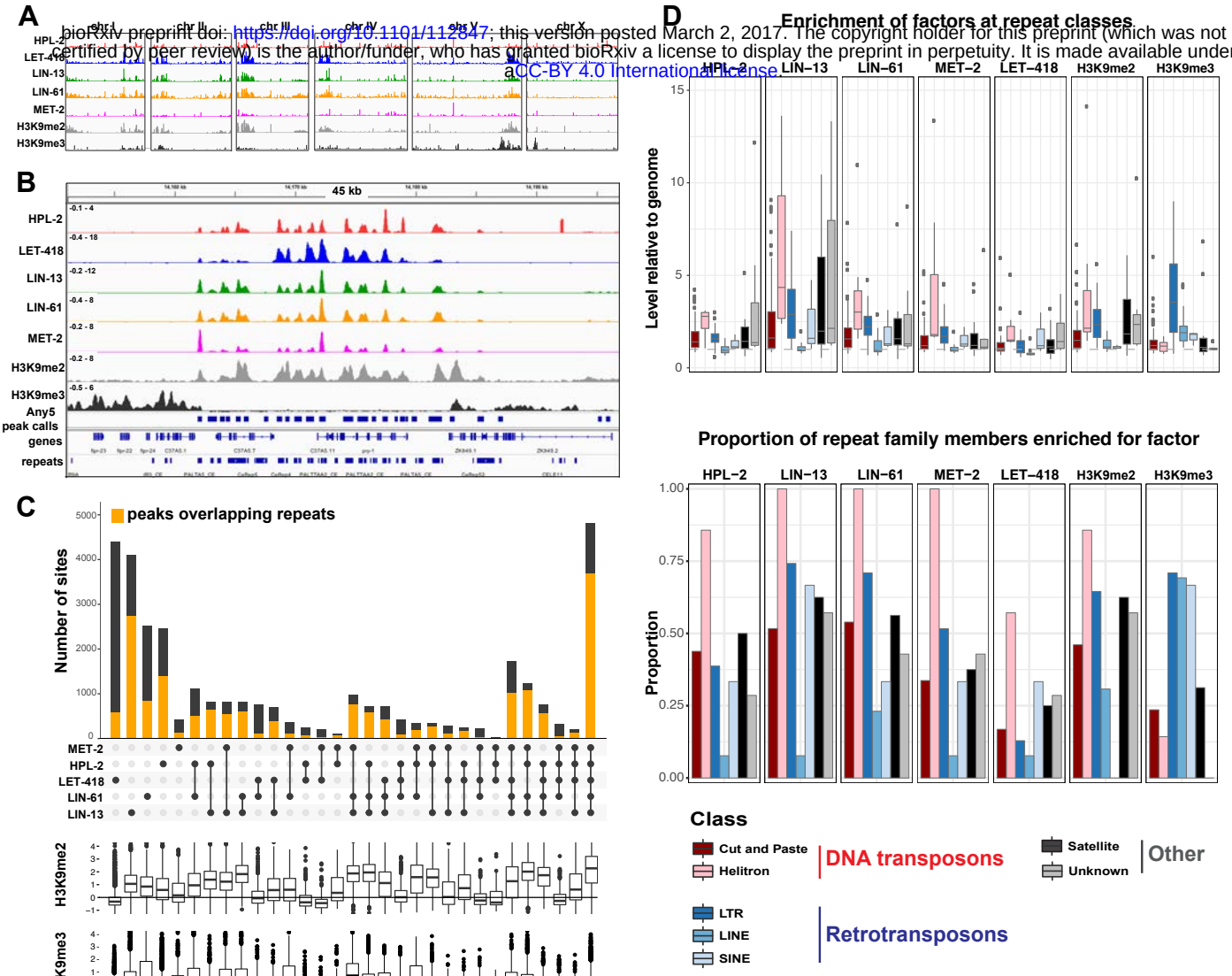

Figure 2

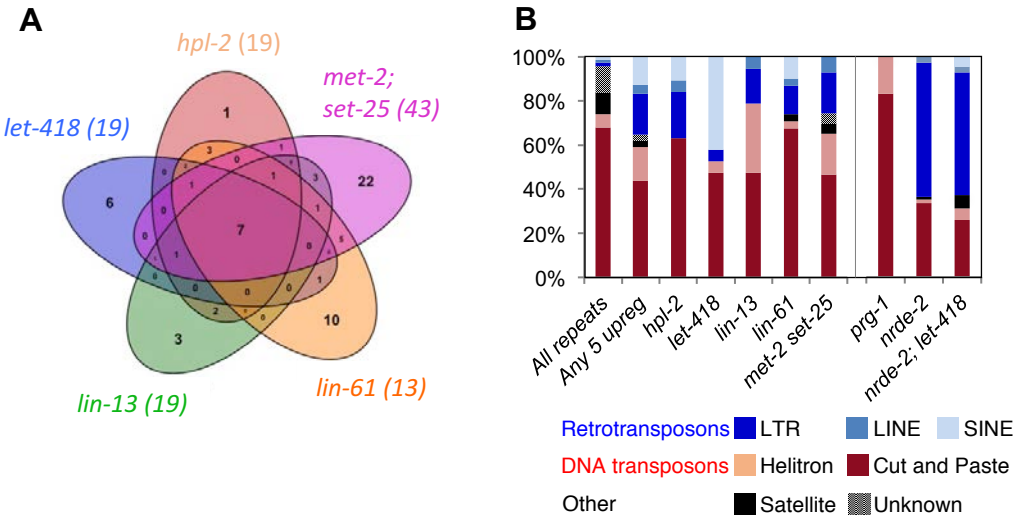

C

Repeat Family	Number of strains upregulating element in family
MIRAGE1	5
Vingi-1_CE	4
CER9-I_CE	4
CERP2	3
Helitron1_CE	3
CELE45	3
CEMUDR1	2
CEMUDR2	2
TC4	2
HelitronY1_CE	2
CER16-2-I_CE	2
CER9-LTR_CE	2
RC35	2
CELE46B	1
HelitronY1A_CE	1
Turmoil2	1
PALTTTAAA2	1
CELE1	1
CELE4	1
CELE14B	1
PAL8C_4	1
CER15-I_CE	1
CER10-I_CE	1
CER1	1
LTRCER1	1
NeSL-1	1
RTE1	1
CERP3	1
CeRep5	1

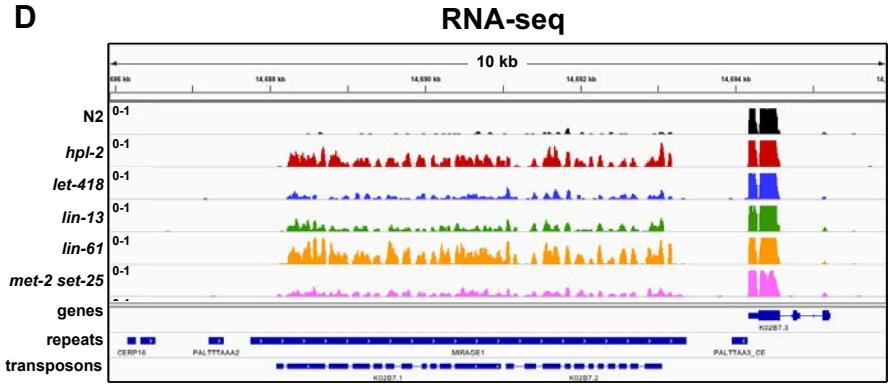

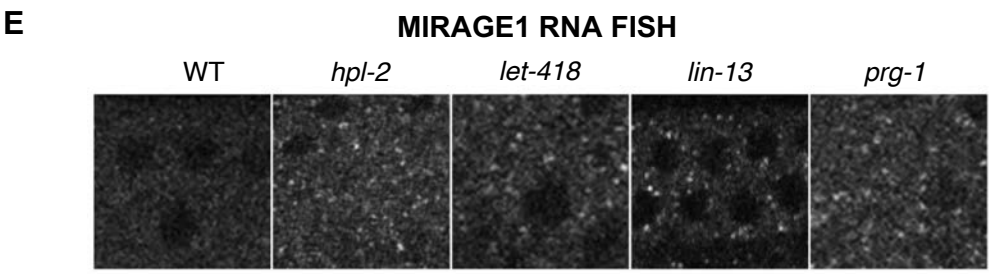

Figure 3

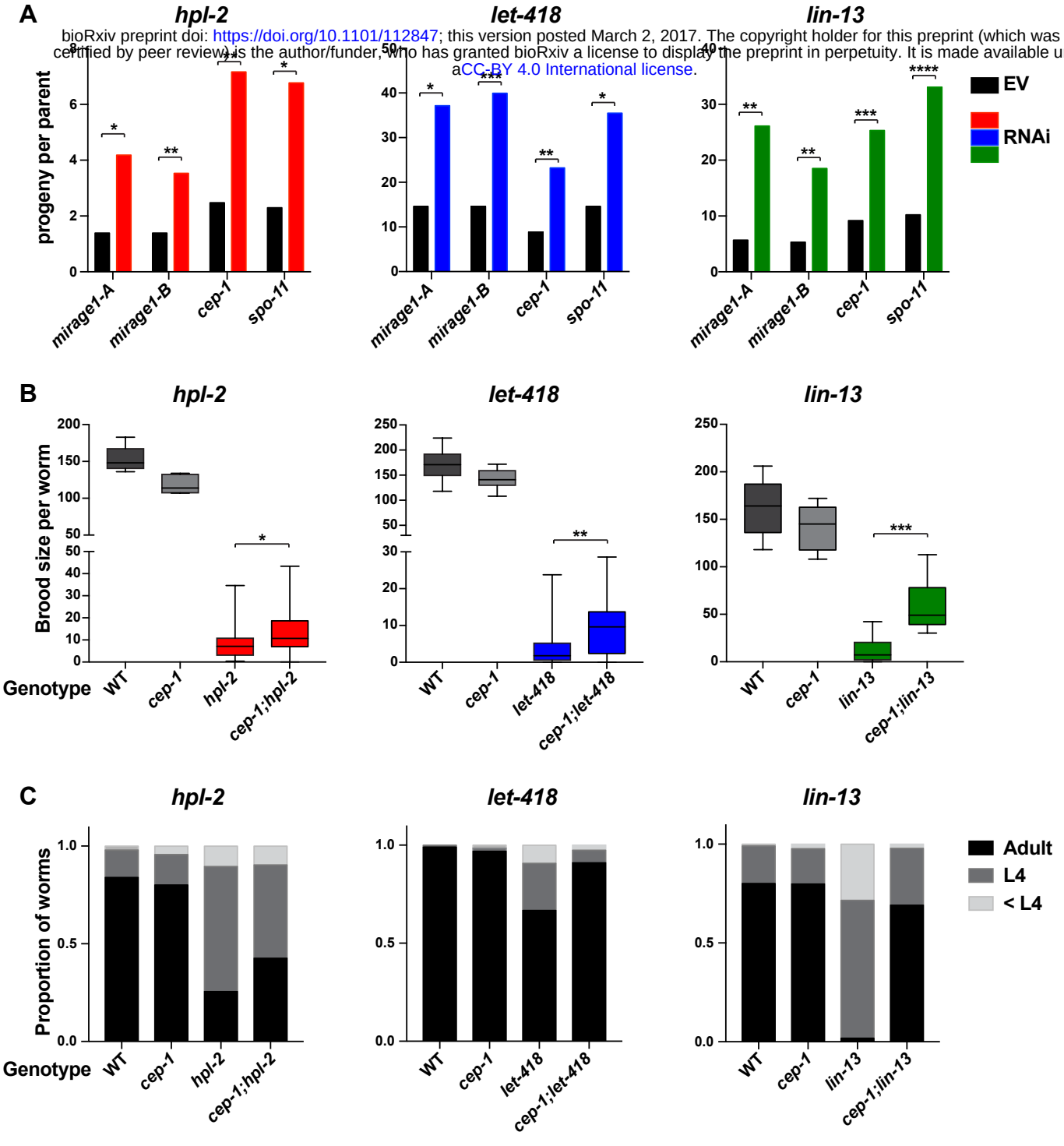

Figure 4

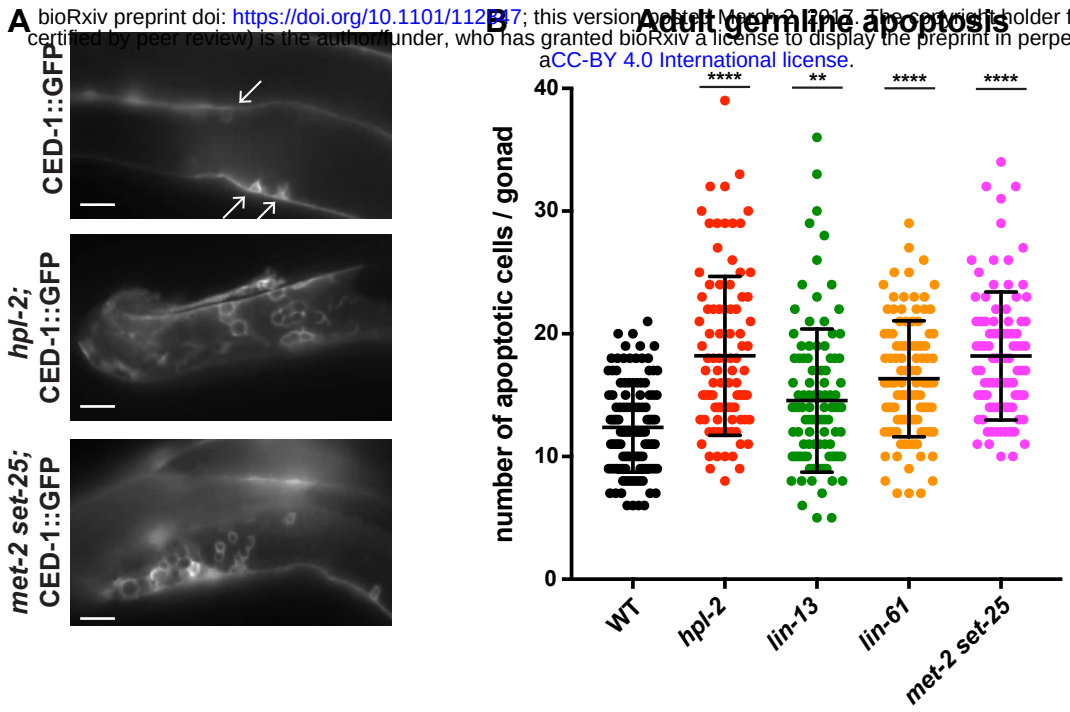

Figure 5

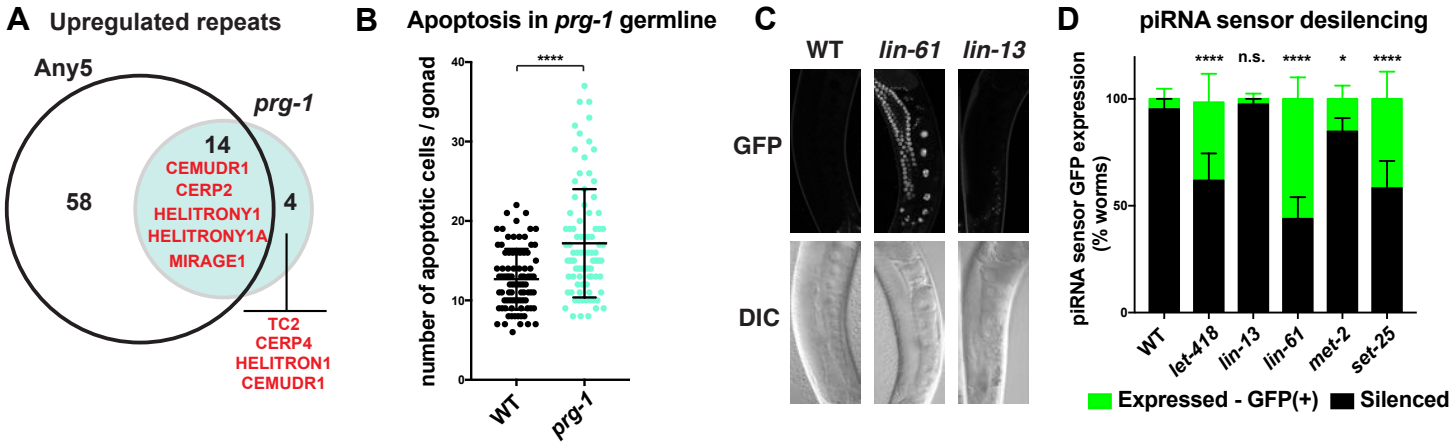

Figure 6

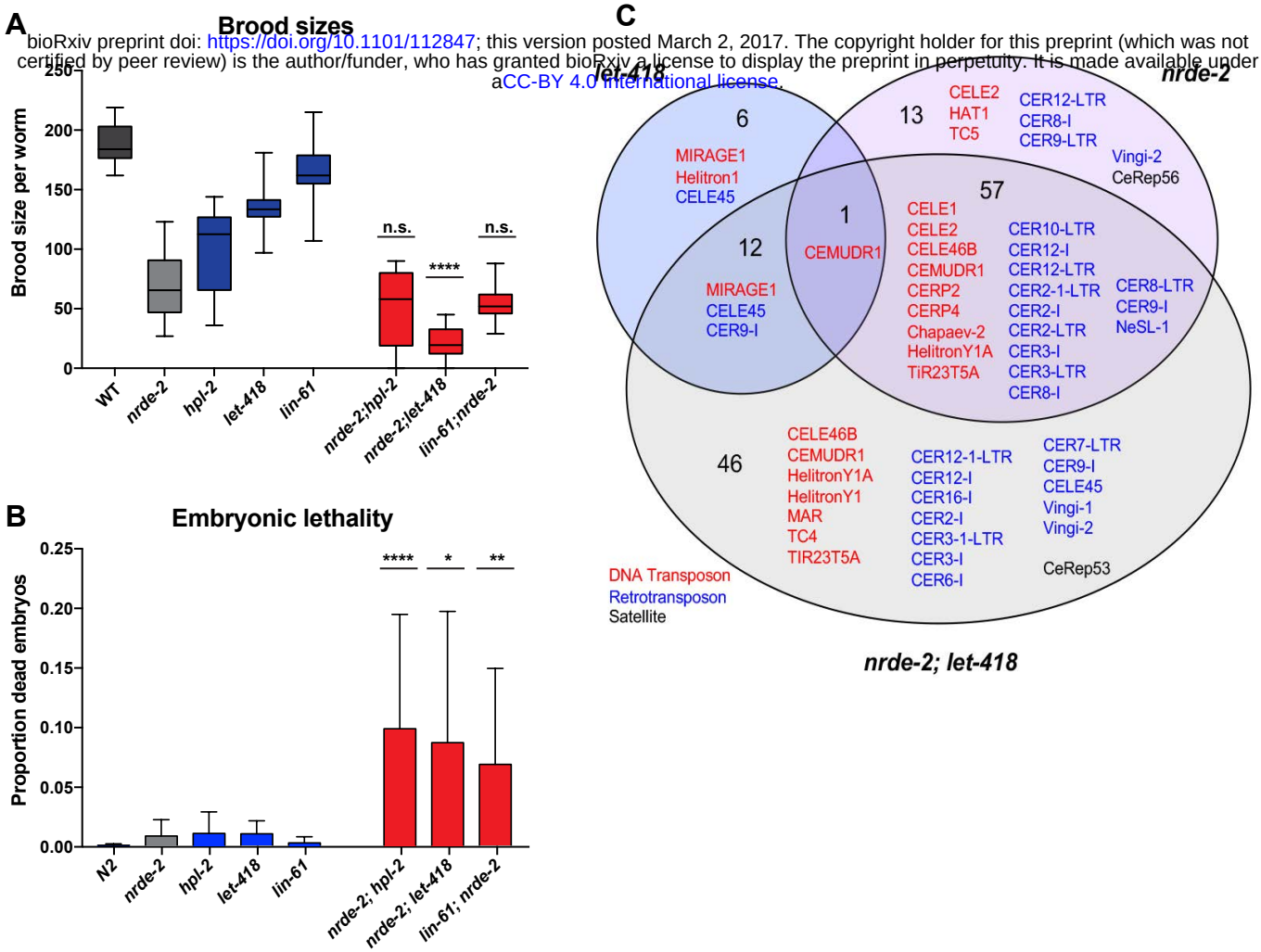

Figure 7

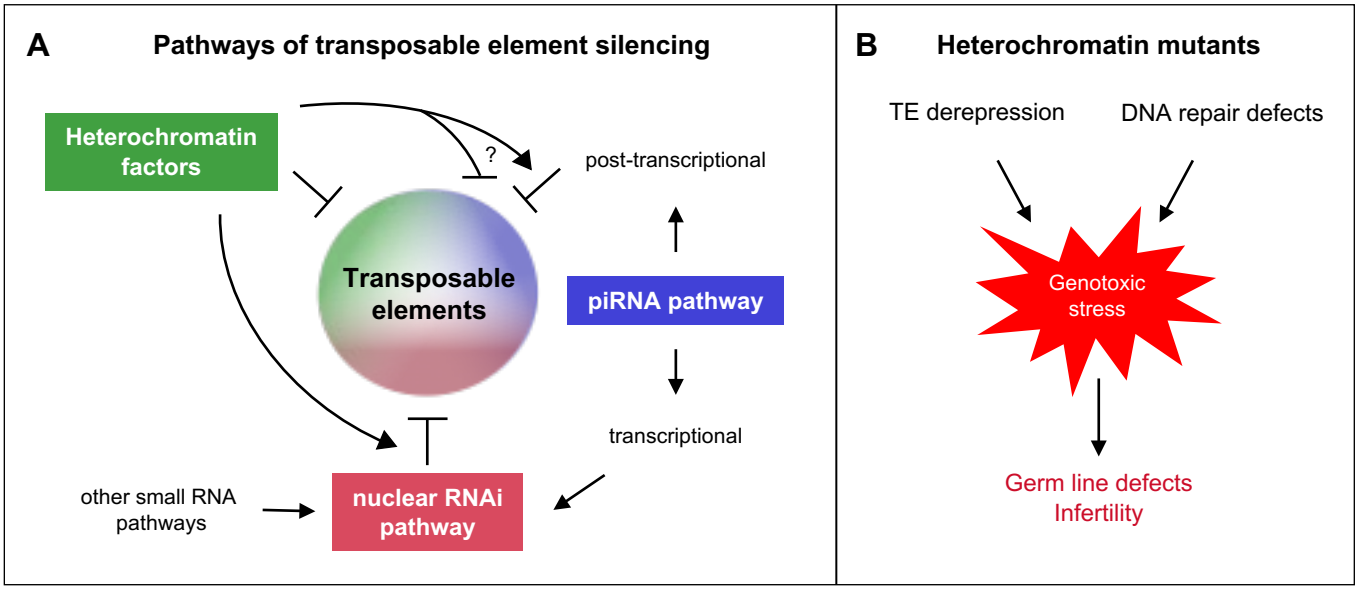

Figure 8